

DESIGNING, IMPLEMENTING AND ANALYZING GRID CONNECTED PV SYSTEMS BY PARTICLE SWARM OPTIMIZATION METHOD

This thesis report is submitted in partial fulfillment of the requirements for the Degree of **Bachelor of Science in Electrical and Electronic Engineering**.

Submitted by

S M Fahim Foyshal Rifad

ID: 182-33-4772

Md. Hasan Molla

ID: 182-33-4612

Misbahul Haq

ID:182-33-4710

Supervised by

Md. Dara Abdus Satter

Associate Professor

Department of Electrical & Electronic Engineering

Faculty of Engineering



Department of Electrical and Electronic Engineering

Faculty of Engineering

DAFFODIL INTERNATIONAL UNIVERSITY

April 2022

CERTIFICATION

This is to certify that this project entitled “**Designing, implementing and analyzing Grid connected Pv Systems by particle swarm optimization method**” is done by the following students under my direct supervision. This thesis work has been carried out by Matlab software of the Department of Electrical and Electronic Engineering under the Faculty of Engineering, Daffodil International University in partial fulfillment of the requirements for the degree of **Bachelor of Science in Electrical and Electronic Engineering**. The presentation of the work was held

Signature of the candidates

S.M. Fahim Foyshal Rifad.

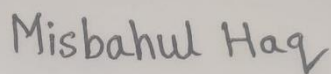
S M Fahim Foyshal Rifad

ID: 182-33-4772



Md. Hasan Molla

ID: 182-33-4612



Misbahul Haq

ID: 182-33-4710

Signature of the supervisor



Md. Dara Abdus Satter
(Associate Professor)

DECLARATION

The thesis entitled “**Designing, implementing and analyzing Grid connected PV Systems by particle swarm optimization method**” submitted by **S M Fahim Foyshal Rifad, ID: 182-33-4772, MD. Hasan Molla, ID: 182-33-4612, Misbahul Haq, ID: 182-33-4710** Session: Summer 2018 has been accepted as satisfactory in partial fulfillment of the degree of **Bachelor of Science in Electrical and Electronic Engineering**.

BOARD OF EXAMINERS

Signature of the supervisor



Md. Dara Abdus Satter
(Associate Professor)

External

Member

Coordinator

Dedicated to.....

OUR BELOVED PARENTS

&

ALL OF OUR TEACHERS

Contents

CERTIFICATION	ii
DECLARATION	iii
LIST OF FIGURES	vi
List of tables	vii
LIST OF ABBREVIATIONS	viii
LIST OF SYMBOLS	ix
ACKNOWLEDGEMENT	xi
ABSTRACT.....	xii
Chapter 1	
1.1 Introduction:	1
1.2 OBJECTIVE WE STUDY:	3
1.3 WHY DO WE PREFER THE SUN AS A NON CONVENTIONAL ENERGY SOURCE? 4	
1.4 Solar Photovoltaic System & Technology:	4
1.5 Photovoltaic Power Generation:	5
Chapter 2	
2.1 Description of the grid-related PV inverter device:.....	7
2.2 PV System Model:.....	7
2.3 DC to DC Boost Converter with MPPT:	11
2.4 DC–AC Inverter:.....	11
2.4.1. Inverter control strategy:.....	12
2.4.2. Phase lock loop:	14
2.5 Voltage regulator controller:	15
2.6 Current controller:	16
Chapter 3	
3.1 PI-based PSO algorithm:	17
3.2 Fault Analyses:	20
Chapter 4	
4. Results and discussion:	23
Chapter 5	
5 Conclusion:	35
References:	38

LIST OF FIGURES

- Fig. 1 Solar PV System
- Fig. 2 Schematic of the grid-connected PV system
- Fig. 3 Equivalent circuit of the PV model
- Fig. 4 Characteristic curves of PV
- Fig. 5 Grid-connected PV system with the three-phase inverter control scheme
- Fig. 6 Block diagram of the PLL
- Fig. 7 The current controller in the grid-connected mode
- Fig. 8 Schematic diagram of the proposed PSO optimization technique for the inverter control scheme
- Fig. 9 Typical-faults-in-a-grid-connected-PV-system
- Fig. 10 Schematic Line to-line fault
- Fig. 11 DC link voltage for both the conventional and optimization methods
- Fig. 12 Three-phase output voltage comparison of the output grid system
- Fig. 13 Three-phase output current for the grid system
- Fig. 14 PI controller
- Fig. 15 THD and harmonic spectrum of the inverter output voltage. (a) Conventional PI controller; (b) PI controller with PSO
- Fig. 16 THD and harmonic spectrum of the inverter output current. (a) Conventional PI controller; (b) PI controller with PSO
- Fig. 17 Relationship curve between fitness function and iteration
- Fig. 18 Frequency response of the grid-connected PV system
- Fig. 19 Active current references i_d of the inverter control system under load variation
- Fig. 20 Active current references i_d of the inverter control system under grid disturbance

List of tables

Table 1	Principal parameters of the PV module
Table 2	Main parameters of the inverter connected grid
Table 3	Advantages and disadvantages of the control algorithm
Table 4	Comparison of the values of the final parameters with different techniques
Table 5	Comparison of reported works

LIST OF ABBREVIATIONS

AC	Alternating Current
ADCs	Analogue-to-Digital Converters
CSIs	Current Source Inverters
DC	Direct Current
FFT	Fast Fourier Transform
HIL	Hardware-in-the Loop
IEC	International Electro-technical Commission
IEEE	Institute of Electrical and Electronics Engineers
IGBT	Insulated Gate Bipolar Transistor
MBD	Model Based Design
MOSFET	Metal-Oxide Semiconductor Field-Effect Transistor
MPP	Maximum Power Point
MPPT	Maximum Power Point Tracker
P&O	Perturb and Observe
PLL	Phase locked Loop
PSO	Particle Swarm Optimization
PV	Photovoltaic
PWM	Pulse Width Modulation
RMS	Root Mean Square
SPWM	Sinusoidal Pulse Width Modulation
STC	Standard Test Conditions
THD	Total Harmonic Distortion

LIST OF SYMBOLS

I	Output current of PV cell (amperes)
V	Output voltage of PV cell (volts)
I_s	Reverse saturation current (amperes)
I_{Ph}	Photo-generated current (amperes)
R_s	Series resistance of the cell (ohm)
R_{sh}	Shunt resistance of the cell (ohm)
N_p	Number of cells connected in parallel
N_s	Number of cells connected in series
I_{sc}	Short circuit current, [A]
K_i	Short circuit current coefficient
V_{oc}	Open circuit voltage, [V]
K_v	Open circuit voltage coefficient
I_{mp}	Current at maximum power
V_{mp}	Voltage at maximum power
V_T	Thermal voltage for PV cell
T	The absolute cell temperature
T_{std}	Standard cell temperature
$T_{std} =$	298 Kelvin
G	Intensity of radiation
G_{std}	Solar irradiance, $G_{std} = 1000 \text{ W/m}^2$
I_{s1}	Saturation current due to diffusion mechanism
I_{s2}	Saturation current due to recombination in space-charge layer
q	Electron charge; $1.6 * 10^{-19} \text{ C}$
k	Boltzmann's constant; $1.38 * 10^{-23} \text{ J/Kelvin}$

E_g	Band gap energy of the semiconductor
D	Duty cycle
V_{out}	Output voltage of DC/DC converter
I_{out}	Output current of DC/DC converter V_{PV} voltage of PV module
I_{PV}	Current of PV module
L	Load inductance [H]
C_{in}	Input capacitor of DC/DC converter [F]
C_{out}	Output capacitor of DC/DC converter [F]
V_{grid}	Grid voltage

ACKNOWLEDGEMENT

As a matter of first importance, we express gratefulness to Allah. At that point, we might want to accept this open door to offer our gratefulness and thanks to our undertaking and task supervisor Md. Dara Abdus Satter, Associate Professor and Associate Head of the Department of Electrical and Electronic Engineering Faculty of Engineering of the Daffodil International University, for being committed to supporting, rousing, and controlling us through this venture. This undertaking isn't possible without his valuable counsel and makes a difference. Likewise much thanks for giving us chance to pick this task.

Apart from that, we would like to thank our entire friends for sharing knowledge; information and helping us in making this thesis a success.

ABSTRACT

Grid-connected photovoltaic (PV), negative intensity, and power devices all share the underlying issues of voltage overshoot, rapid reaction, and lack of control over constant error. Delivers the finest results with general damage as well. The effectiveness of an inverter control strategy for a three-phase grid-connected PV device is discussed in this publication. PV panels, boost converters, DC links, inverters, and resistor-inductor (RL) filters make up the machine, which is connected to the utility grid by power inverters. By optimizing the proportional vital (PI) controller, the suggested technique aims to increase the robustness and good performance of the three-part grid-coupled inverter device. This type of approach seeks to stabilize output edges, voltage, frequency, and energy waves while reducing harmonics and DC input voltage variations. To reduce the inaccuracy of the voltage regulator and cutting-edge regulator schemes inside the inverter device, we tracked the PI controller settings by using a particle swarm optimization (PSO) technique. The Sims Cape Energy Device Toolbox in the MATLAB/Simulink environment (model 2021B) was used to apply machine versions and control approaches. With total harmonic distortion (THD) at source voltage and time values of 0.29% and 2.72%, respectively, and a temporal response time of 0.1853 s, the results demonstrate that the proposed technique performs better than prior research that have been discussed. This PSO-based global optimization PI regulator drastically reduces voltage overshoot by 11.1% when compared to conventional systems, while also slashing the time it takes to attain equilibrium by 32.6%. First-class power control has significantly improved as a result of paying attention to additional input parameters and optimizing input parameters.

CHAPTER 1

INTRODUCTION

1.1 Introduction:

Significant problems with air pollution, climate change, and global warming have an impact on both natural resources and human health. The cost of putting off solving these problems today may be much greater than the likelihood of success down the road. As a result, investments in clean energy sources, such as renewable energy, are increasing globally. Photovoltaic (PV) power is anticipated to have a favorable effect on the environment as a renewable energy source with a consistent capacity to supply present and future energy needs. PV modules adopt allocated technology (DG) technology because of their widespread use in power equipment applications and their ability to operate independently of the main grid. This DG unit has undergone extensive development in a number of nations, including Spain, Germany, Japan, and the USA [1]. For PV devices fed to the grid via inverters, the primary issues are high power quality, balance, and performance disparities. When converting renewable modern direct (DC) power into modern (AC) power for AC ground or delivering energy to the software grid, inverters consume electricity. It is an electronic gadget [2].

Inverter management needs to be done properly while using PV energy. This is due to the fact that PV power devices become highly desirable to consumers, especially in situations where they are not already available. A contemporary control technique is in charge of one of these devices' large-scale grid-connected PV machine power supply. This method includes the use of a proportional-integral (PI) controller that is forced. We are all aware that PI controllers are widely employed in several programs and gadgets due to their straightforward operational structure, slick construction, minimal power consumption, and consistent overall performance [3, 4]. It can resolve a variety of issues for different programs, including: B. Excessive overshoots, typical mistakes, and fluctuations brought on by system fluctuations. The parameters of the PI controller must be accurately received in order to ensure correct functionality and robust control of the operation loop device [5].

Preferable tuning techniques, such as Ziegler-Nichols, Cohen-Coon, and self-tuning fuzzy PI-based M-constrained gain-of-needs optimization (MIGO) [6,7], can be used to find comfortable settings for the PI controller parameters. However, a weak technical foundation of mathematical iterations and trial-and-error results in a less reliable controller that produces subpar outcomes. Additionally, a sliding mode controller (SMC) was developed to fix the inverter output voltage's periodic inaccuracy as the load varies. Its THD for linear and nonlinear loads is reduced to achieve the desired results [8]. To further enhance the performance of the PI controller, numerous optimization techniques like genetic algorithms (GA), particle swarm optimization (PSO), differential evolution (DE), ant colony optimization, and neural fuzzy evaluation are also used. That variable has been altered. [9-11]. we concentrate on the GA implementation in back-propagating neural networks for PID controllers in order to optimize the initial weights and reduce the DC contemporary [12]. The difficulty of achieving the web optimization process is demonstrated by GA optimization, which demonstrates that by investing more time in the optimization process, the total performance within the DC contemporary suppression process is enhanced. increase. However, compared to the GA approach, the PSO algorithm can produce an optimal response in less time due to its single search range for the solution. Additionally, the Ant Colony Algorithm (ACA) was employed in several other research to enhance his PI settings for backup PV arrays [13]. The Jaya algorithm is also tuned to minimize frequency deviation in hybrid electric vehicle (HEV) packages using PID controllers [14]. To verify the efficiency of the algorithm, one observer applied optimization of the Jaya algorithm inside the parameter estimation of soil water retention [15]. Similar to this, the BAT algorithm was applied to all other paintings [16] in order to find the best settings for her PI controller for PV devices that are connected to the grid. Because of its benefits, including robustness and global convergence ability, clean implementation, and ease of calculation, the PSO method is frequently utilized in optimization solutions [17, 18]. Additionally, the PSO rule set was able to arrive at the most secure solution faster than the GA method. This research have has own that the design of the best-in-class Her PI controllers for energy converters in DG structures is largely dependent on optimization procedures.

Thus, in today's talk, PSO is employed for the crucial PI controller parameter design. This seeks to enhance the power and stability of three-phase grid-connected PV inverter devices while maintaining the quality and best K_p and K_i values in actual operation.

Two PI controllers are used with a synchronous reference body to implement the suggested control strategy. To produce excess dynamics, a feedforward payback is used in the inverter's inner peak control loop. In light of the comments just made, the aforementioned references have inadequate process facts, are less resilient, take longer to compute than PSO, handle parameter complexity, and have exceptionally high fitness costs for finding. There are restrictions on the coding problems of Inverter optimization's effects on improving energy efficiency, lowering DC link voltage fluctuations, stabilizing output current and voltage, easing energy flow, reducing harmonics, and stabilizing frequency inside the grid-related PV inverter are also not properly covered. As a result, this work aims to improve the inverter system's energy efficiency by reducing temporary response, limiting time overshoot, and achieving low constant-country errors due to the model in.

Along with DC link stability, hundreds. Similar to this, the PSO is employed to obtain the most ideal values of the PI management parameters, reduce error, and improve the voltage and frequency balance in a quicker and less difficult manner. The (m-record) code in MATLAB is used to complete the PSO algorithm's implementation, and MATLAB/Simulink is utilized to develop the inverter control scheme with a 3MW PV electricity generation.

The simulated results show that, in comparison to the PI controller without the optimization method, the PI controller with the optimization strategy offers excellent overall performance with little variance in overall harmonic distortion (THD).

1.2 OBJECTIVE WE STUDY:

1. To get the best quality values of the controller, we suggest an optimized PSO rule set. A three-part grid-connected PV inverter's intensity quality and balance are improved by K_p and K_i working in real-time.
2. To reach the ultimate optimization of the PI controller parameters, reducing transient responses, minimizing timeouts, and attaining low variant-induced errors in the steady-state area must be accomplished. Maintain the cost. Loading progress.
3. By reducing mistakes as much as possible and using load transient situations to find the best and most informative PI controller parameters, provide real-time operation of PV inverter devices with optimized controllers.

1.3 WHY DO WE PREFER THE SUN AS A NON CONVENTIONAL ENERGY SOURCE?

There are numerous unorthodox energy sources, such as solar heat, wind power, ocean tides, and geothermal energy. Every atypical strength has a defined geographic range. Solar energy is less expensive than other unconventional energy sources due to the fact that it is accessible everywhere in the world and that the size of the collector object is all that is required to produce the same quantity of heat or energy. less geographic limitations Finding the quantity, quality, and timeliness of solar energy at a potential location for solar energy converter installation is the main responsibility of a solar energy system developer. This offers humanity the most potential of all the solar energies. It is uncontrollable, limitless, eco-friendly, and unaffected by political manipulation. Solar panel heaters, stoves, and water heaters are already available and seem to be financially realistic options. Solar freezers, solar power plants, and solar image Volta cells will soon be economically and technically possible. By the middle of the twenty-first century, it is anticipated that solar energy alone would be able to supply 50% of the world's electricity demands. To avoid the transfer of thermal energy to mechanical energy, the direct power conversion system was extended during the past two years. This increased plant performance by 60% to 70%. Nevertheless, technology is poised for success and is anticipated to be crucial in the next electric age.

1.4 Solar Photovoltaic System & Technology:

Systems and technologies for converting sunlight directly into electricity without the use of a heat output interface are known as photovoltaics. The photovoltaic system's architecture is straightforward, durable, and low-maintenance. The main benefit of this solar power system is that it can produce power ranging from megawatts to microwatts and is designed as a standalone system. They are utilized in power sources, solar-powered homes, water pumps, communications, satellites, and spacecraft because of this. Additionally, megawatt-scale power plants make use of it. The demand for this photovoltaic system is rising as a result of its numerous uses.

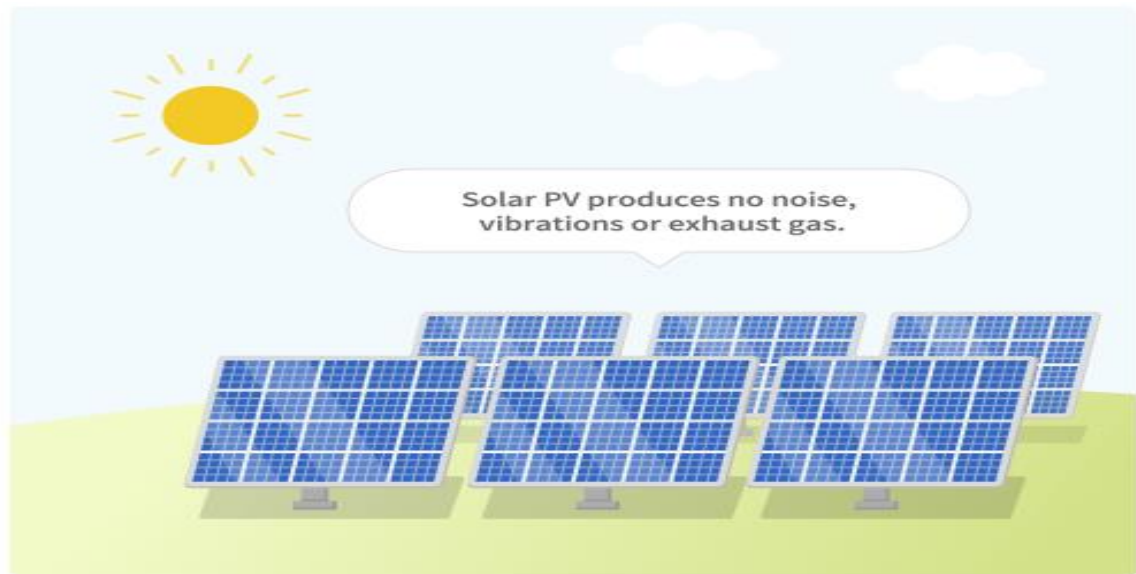


Fig1: Solar PV System

1.5 Photovoltaic Power Generation:

(See further) A photovoltaic system is made up of a variety of parts, including cells, supports, mechanical and electrical connections, and devices for controlling or modifying the electrical output. The system is primarily rated in peak kilowatts (kWp). Peak Kilowatt (kWp) is the precise amount of power anticipated to be delivered on a clear day when the sun is overheating. Grid-tied PV systems are typically connected to sizable portions of an independent power grid, which receives its energy from the utility grid. Residential solar power systems up to 10 GWp use kWp. Distributed generation is what is being used here. Poponi estimated the rate of power generation in grid-connected systems using the empirical curve approach, which is used to forecast the various amounts of accumulated global PV supply necessary to reach the determined break-even point. to determine PV pricing and the likelihood of photovoltaic (PV) technology adoption. a model that takes into account various trends in the relationship between rising pricing and supply over time [1 pv]. Ito et al. The energy payback time (EPT), life of the complete cycle, and CO₂ emission rate were evaluated for a 100 MW very large scale photovoltaic (VLS-PV) system that would be deployed in the Gobi Desert. We assessed its potential in terms of the economy and the environment. Cost of system generation [4]. within et al. By examining the cash flows generated over the course of a 100 MW power plant's lifetime, an economic analysis of power generation from a floating updraft power plant (FSCPP) was carried out [5]. In arid and semi-arid regions of the world, Mounir et al. evaluated the long-term prospects for large-scale PV power generation and its transmission utilizing hydrogen as an energy carrier [6]. In

terms of system technology and components employed, management, and prices, Snow et al. described the megawatt system at the new Munich Trade Fair Center as a substantial advancement in large-scale photovoltaic system technology. 7].

CHAPTER 2

DESCRIPTION AND OVERVIEW OF PV SYSTEM

2.1 Description of the grid-related PV inverter device:

A three-segment voltage supply inverter (VSI) is utilized in Figure 1 to depict a grid-tied PV system. PV arrays, MPPTs (maximum power factor monitors), controllers, inverters, filters, and loads are all included in this. The output of the PV device is linked to a DC hyperlink capacitor, and the output becomes the input voltage of the inverter device. Utilize a boost converter and MPPT rule set to get the most power possible out of a PV device. To power, the loads, a step-up transformer on the distribution side connects a three-phase VSI with control and RLC filtered outputs to the low-voltage AC grid. Below is a description of a precise dynamic model of a grid-connected PV equipment.

2.2 PV System Model:

The basic part of a PV machine is known as a solar cell. Several individual solar cells connected in series form a PV module [17, 18]. Synchronization of PV modules,

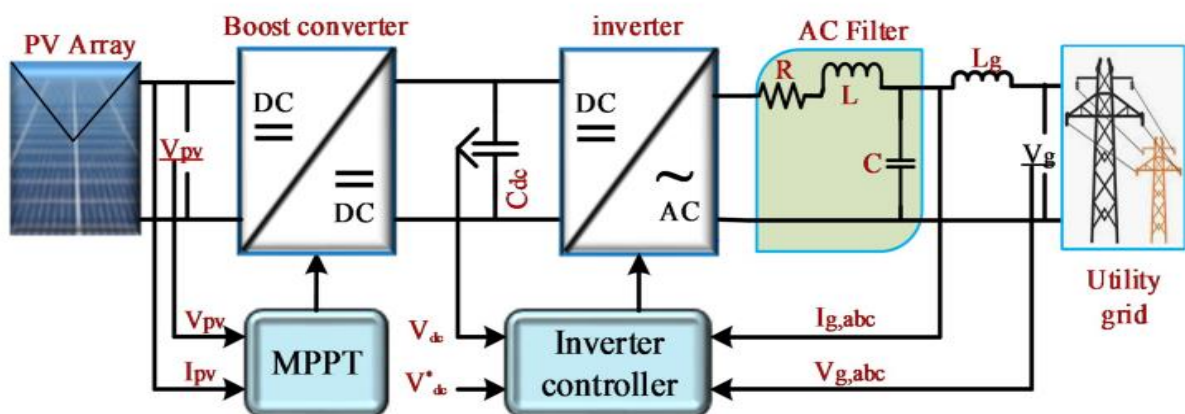


Fig2.Schematic of the grid-connected PV system.

As shown in Figure 2, it consists of a photocurrent supply I_{ph} , a parallel supply diode (D), a collection resistor R_s , and a shunt resistor R_{sh} placed in parallel with the diode. Based entirely on the equivalent circuit, the relationship between output voltage and current

equation (1) is expressed as [18, 19].

$$I_{pv} = I_{ph} - I_{sh} \left(\exp \left(\frac{V_{pv} + IR_s}{AN_sKT} \right) - 1 \right) - \frac{V_{pv} + IR_s}{R_{sh}} \quad (1)$$

where I_{ph} is the photocurrent, I_{sh} is the current saturation, A is the perfect diode component, q is the electron charge (1.602×10^{-19} C), k is the Boltzmann constant (1.381×10^{-23}), T is the transfer Body. N_s are various PV cells connected in series. The photocurrent of a PV cell at any irradiance and temperature can be calculated using equations (2), (3), and (4).

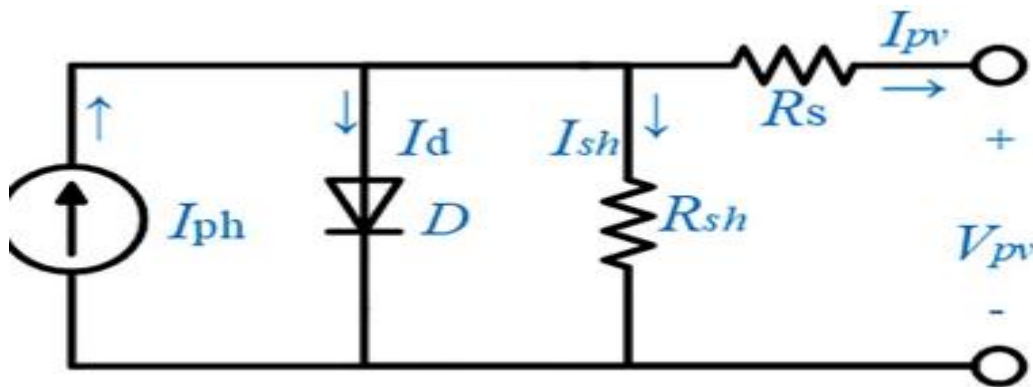


Fig3. Equivalent circuit of the PV model

Table1. Principal parameters of the PV module.

Parameters	Value
Maximum power	$P_{max} = 213w$
Maximum power voltage	$V_{mp} = 29.52v$
Maximum power current	$I_{mp} = 7.28 A$
Open-circuit voltage	$V_{oc} = 36.48 V$
Short-circuit current	$I_{sc} = 7.79A$
Cell number per module	$N = 60$
Temperature coefficient of I_{sc}	$K_i = 0.054/^{\circ}C$

Temperature coefficient of Voc

$$K_v = -0.353/^\circ\text{C}$$

Ideality factor of the diode

$$A = 0.972$$

$$I_{ph} = \frac{G}{G_{ref}} * [I_{sc} + K_i(T - T_{rk})] \quad 2$$

$$I_{sc} = I_{sc.ref} \left(\frac{R_p + R_s}{R_p} \right) \quad 3$$

$$I_{sc} = \frac{I_{sc.ref} + K_i(T - T_{rk})}{e^{q\left(V_{oc.ref} + \frac{K_v(T - T_{rk})}{AN_sKT}\right)} - 1} \quad 4$$

G_{ref} and G are the nominal and real solar irradiation, respectively; T_{rk} is the module Absolute Kelvin scale of temperature. K_i is the trip current's temperature coefficient. The open circuit voltage's temperature coefficient is denoted as K_v . I_{sc} , $I_{sc.ref}$, and V_{oc} are additional terms, where $I_{sc.ref}$ denotes the modules short-circuit current and open-circuit voltage under predetermined test conditions [21]. Based on equations (1) to (2), Table 1 displays the parameter values for PV modules (4). The P-V and i-V characteristic curves are determined by the Simulink version using the same test, based on the mathematical form of the PV module above. According to Figure 4.

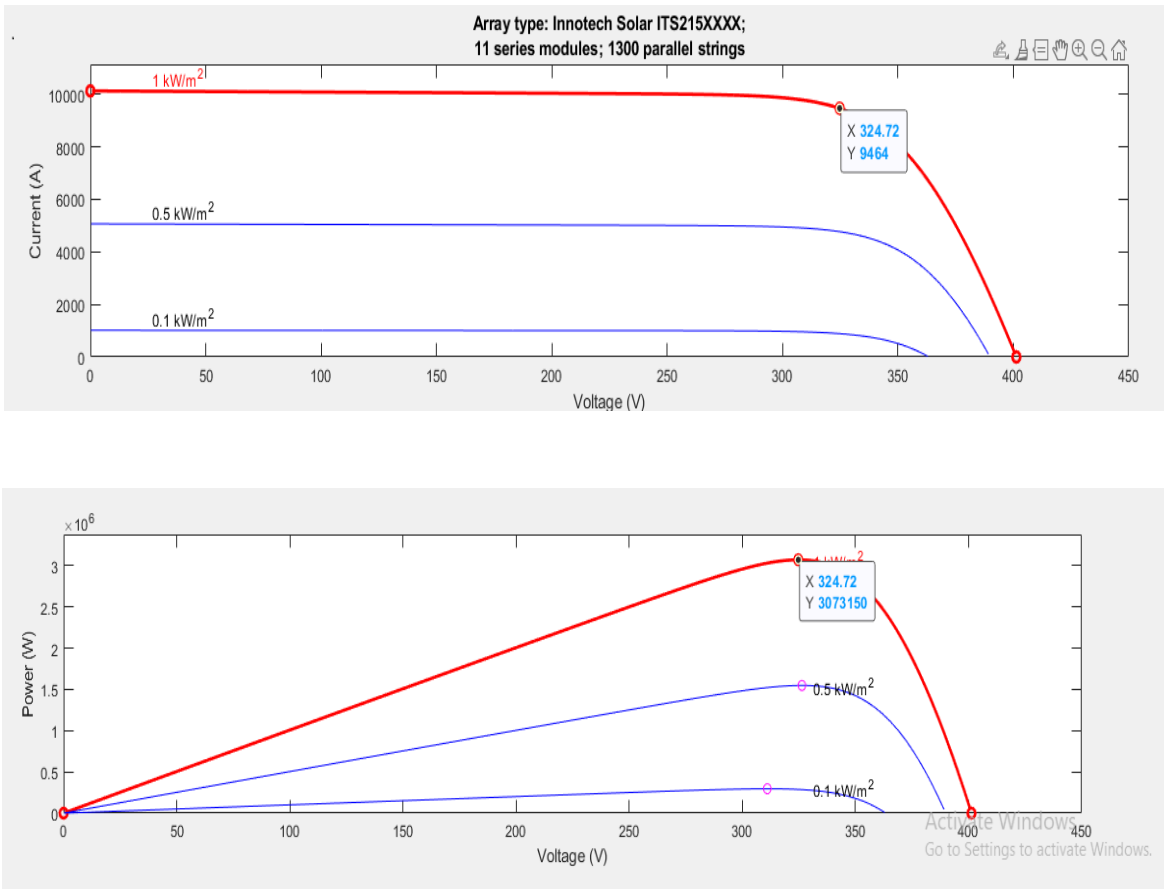


Fig4. Characteristic curves of PV

2.3 DC to DC Boost Converter with MPPT:

With a lower input voltage, a boost converter (DC to DC) typically generates a higher output voltage. When a larger output voltage is needed, use. B. Due to non-minimum phase behavior, control design for DC-DC boost converters, such as solar panels, wind turbines, and electric cars, is challenging. Typical curves for various areas of solar radiation and photovoltaic systems. Figure 4 illustrates [3]. The voltage and current of PV arrays are significantly impacted by non-linear changes in solar irradiation and temperature, leading to unpredictable power availability [22]. To track the maximum power from the PV array based on the irradiance and temperature levels produced, the MPPT method, also known as Peer and Observe (P&O), is employed in this system together with a DC-DC boost converter. In [23, 24], a detailed description of MPPT approaches and algorithms may be found. The P&O approach is used by the system. PV voltage V_{pv} and PV power are detectable, and I_{pv} controls the maximum PV power. By adjusting the duty cycle D of the PWM components in the advanced inverter, the extracted PV voltage is raised to 500 V relative to the DC voltage V_{dc} . People with PV systems that are connected to the grid have an intermediary circuit. To eliminate the current output ripple and to control and stabilize the voltage on the DC side of the line converter, the DC link should have a value that is near to the maximum array voltage. To get the most out of different inverter voltages, inverters should be well-matched to contemporary array voltages. The rated voltage of the inverters is same because of the DC link. This boost DC/DC boost converter's formula is:

$$V_{dc} = \frac{V_{pv}}{1 - D} \quad 5$$

2.4. DC–AC Inverter:

An inverter reduces high frequency harmonics to the line machine by converting DC power to AC power through an AC filter output [25]. The controller generates PWM pass/fail signals for converter transmission in accordance with the output characteristics and control strategy of the converter. FIG. depicts a block diagram of the inverter operating system in normal operation. It is made up of a filter, an insulated gate bipolar transistor (IGBT), and a hyperlink DC voltage. The input DC link, which helps to stabilize the input voltage fed to the inverter, is made up of a 1200 F capacitor linking the DC power source to the inverter machine. To cut down on excessive frequency

harmonic components supplying the grid system, the inverter is connected to the grid through an AC filter [26]. A voltage operating loop and an internal modern loop make up the inverter operating machine. While stabilizing and controlling the DC link voltage V_{dc} in the voltage loop, a PI regulator in the inner modern loop assists in changing the main modern and DC hyperlink voltages [19,24].

$$\begin{matrix} V_{od} \\ V_{oq} \\ V_0 \end{matrix} = \sqrt{\frac{2}{3}} \begin{pmatrix} \cos \theta & \cos(\theta - 2\pi/3) & \cos(\theta + 2\pi/3) \\ -\sin \theta & -\sin(\theta - 2\pi/3) & -\sin(\theta + 2\pi/3) \\ 1/2 & 1/2 & 1/2 \end{pmatrix} \begin{pmatrix} V_{ga} \\ V_{gb} \\ V_{gc} \end{pmatrix} \quad 6$$

2.4.1. Inverter control strategy:

A segment-locked loop (PLL), which is essentially based on the usage of a synchronous direct quadrature (d-q) reference and the Park transform, is used to synchronize line voltage and phase. The d-q rules are straightforward and exhibit excellent dynamic responses [27]. By integrating the reference angular frequency, the reference angle is determined. Grid voltage V_g , ABC and grid current I_g , ABC are transformed from ABC to d-q using the crossing angle derived from the PLL to produce the voltage and current, respectively, in the d-q axis reference body. Equations (6) and (7) are used to convert the values measured in percent to the d-q axis reference object [28].

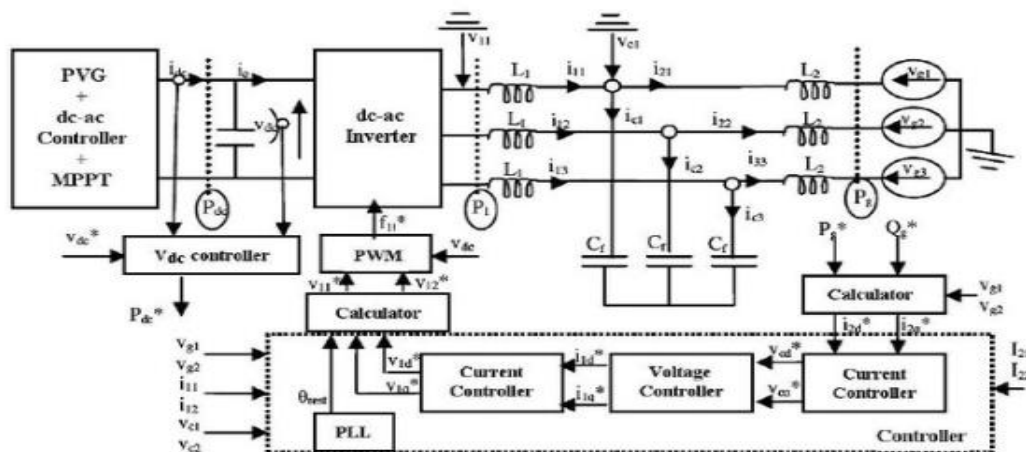


Fig5. Grid-connected PV system with three-phase inverter control scheme.

$$\begin{matrix} i_{od} \\ i_{oq} \\ i_o \end{matrix} = \sqrt{\frac{2}{3}} \begin{pmatrix} \cos \theta & \cos(\theta - 2\pi/3) & \cos(\theta + 2\pi/3) \\ -\sin \theta & -\sin(\theta - 2\pi/3) & -\sin(\theta + 2\pi/3) \\ 1/2 & 1/2 & 1/2 \end{pmatrix} \begin{pmatrix} I_{ga} \\ I_{gb} \\ I_{gc} \end{pmatrix} \quad 7$$

where (V_{ga} , V_{gb} , and V_{gc}) and (I_{ga} , I_{gb} , and I_{gc}) are the grid's three-phase voltages and currents, and V_{od} , i_{od} , and V_{oq} are the voltages and currents in the d-q axis reference frame. The internal inverter management controller for the d-q version works with an asymmetric DC charging device ended by a PI controller, therefore the conversion from ABC to d-q is crucial for inverter operation. For the d-q to ABC conversion, which results in V_{ac} , a PI controller in the inner loop creates the active reference voltage V_d and the reactive reference voltage V_q . Within the inner-loop operation, the active and inactive current axis should be distinguished using a feed-ahead term [29]. The PWM character will then use the V_{abc} value to modify the gate pulse for the inverter. Equations (8) and (9) can be used to get the actual response intensity after the Park transformation [19, 26]

$$P = \frac{3}{2}(V_{od} * i_{od} + V_{oq} * i_{oq}) \quad 8$$

$$Q = \frac{3}{2}(V_{oq} * i_{od} - V_{od} * i_{oq}) \quad 9$$

where on the d-q axis reference frame of the grid view, V_{od} , V_{oq} , and i_{od} are referred to as tension and cut, respectively. The inner control loop of the inverter control scheme uses advanced control to precisely track the current signal while temporarily removing high-speed hardware. The line-side inverter output energy and reactive voltage (V_d and V_q) for the d-q synchronous body at road frequency can be represented using equations (10), respectively, from the current inner-loop control of the inverter shown in Figure 5. (11).

$$V_{od}^o \rightarrow -i_{od} \left(K_{pq} + \frac{K_{id}}{s} \right) - w * L_f * i_{oq} + V_{od} \quad 10$$

$$V_{oq}^o \rightarrow -i_{oq} \left(K_{pq} + \frac{K_{iq}}{s} \right) - w * L_f * i_{od} + V_{oq} \quad 11$$

Then, utilizing controlled pulses from the inner control loop and the specified amount of current, it turns the VSI inverter. This can be used to supply first-rate, premium power to electrical equipment. The primary characteristics of the grid-connected inverter device are listed in Table 2. More comprehensive statistics about inverter management devices for the grid are provided in [27,28]. In order to deliver premium super energy, the VSI inverter is replaced and fed by a regulated pulse from the inner loop that is operated with a controlled amount of energy. Table 2 displays the major characteristics of the grid-connected inverter device. [27, 28] provide more statistics on grid-connected inverter-operated equipment.

2.4.2. Phase lock loop:

Inverters that are connected to the grid can accurately and quickly detect supply segment settings thanks to the PLL device in Figure 4 [27]. A synchronous PLL frame's

$$\omega = K_p^{PLL} V_{aq} + K_i^{PLL} \int_0^t V_{aq} dt \quad 12$$

$$\theta = \int_0^t \omega dt \quad 13$$

block diagram is shown in FIG. 6. In order to reduce rotation frequency setting errors, the PI controller adjusts V_{oq} to zero. By integrating the angular frequency, the junction point's location is discovered, and it may be written as [29, 30].

Table 2. . Main parameters of the inverter connected grid.

Parameters of the inverter	Value
Effective voltage of the grid	$V_{grid} = 33 \text{ kV}$
DC link voltage	$V_{dc} = 500 \text{ V}$
DC link capacitor	$C_{dc} = 1200 \text{ } \mu\text{F}$
Grid frequency	$\omega = 2\pi * 50 \text{ rad/s}$
R filter of the inverter	$R_f = 1.89 \text{ m}\Omega$
L filter of the inverter	$L_f = 250 \text{ } \mu\text{H}$
Switching frequency of the inverter	$f_s = 2 \text{ kHz}$
Line Resistance	$R_g = 0.04 \text{ } \Omega/\text{km}$
Line Impedance	$X_g = 0.13 \text{ } \Omega/\text{km}$

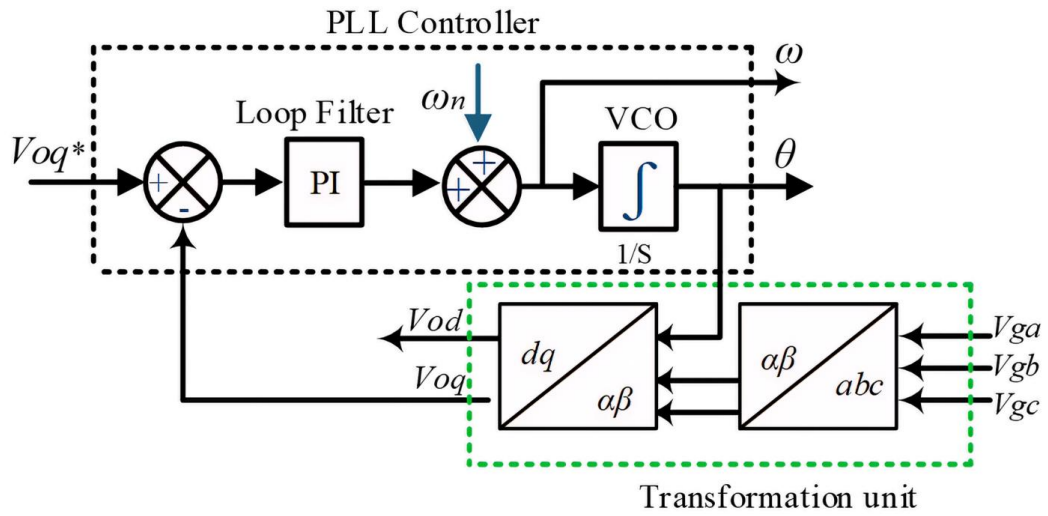


Fig6: Block diagram of the PLL

2.5 Voltage regulator controller:

In grid-connected PV systems, DC linkages play a significant role. They function because the DC bus connects the boost converter and the inverter. A DC link capacitor is a component used to increase the power requirements' convenience and safety [29]. Utilizing a connection controller will allow you to modify the energy slip of your network system. The current discrimination at the grid reference level is produced by a PI controller. As a result, the internal regulator loop's input is changed from the external voltage regulator's output. Equation provides the model for the DC link voltage regulator (14).

$$i_d^o = e * (K_{pdv} + \int K_{idv}) \quad 14$$

where e is the variance between the reference voltage and the voltage being measured. To maintain the DC hyperlink voltage with the least amount of error, the estimated error is the input to the PI controller. The boost converter and the inverter device should have a consistent DC connection voltage. This is because THD, which results in horrific sizes that are at ease on grid devices, is caused by variations over DC connections [31].

2.6 Current controller:

For grid-connected businesses to achieve world-class power improvements, modern regulators are essential. As shown in Figure 7, the current regulator is constructed using a feed-ahead decoupling strategy to the terminal voltage. Modern synchronous d-q frame management necessitates the use of a PLL to detect the viewpoint of the line voltage section if the park transformation is imposed in accordance with equations (6) and (7) [32]. Figure 7 displays a block schematic of a contemporary controller..

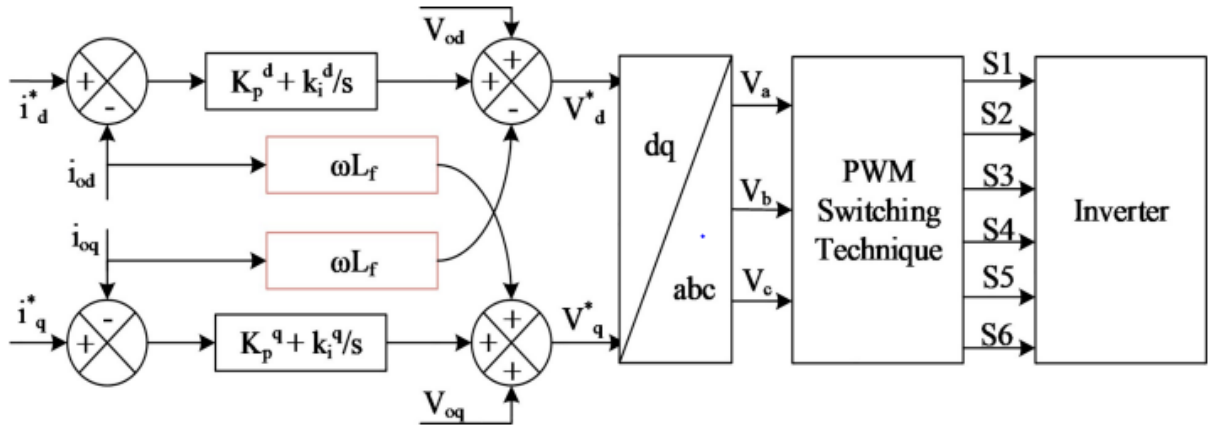


Fig7. The current controller in the grid-connected mode.

From Fig 7, the following equation can be obtained:

$$\begin{bmatrix} V_{od} \\ V_{oq} \end{bmatrix} = \begin{bmatrix} -K_p^d & -\omega L_f \\ \omega L_f & -K_p^d \end{bmatrix} \begin{bmatrix} i_{od} \\ i_{oq} \end{bmatrix} + \begin{bmatrix} K_p^d & 0 \\ 0 & K_p^d \end{bmatrix} \begin{bmatrix} i_d^* \\ i_q^* \end{bmatrix} + \begin{bmatrix} K_i^d & 0 \\ 0 & K_i^d \end{bmatrix} \begin{bmatrix} x_d \\ x_q \end{bmatrix} + \begin{bmatrix} V_{od} \\ V_{oq} \end{bmatrix} \quad 15$$

$$\text{Where, } x_d = (i_d^* - i_{od})/s \quad 16$$

$$x_q = \frac{-i_{oq}}{s} \quad 17$$

In order to feed into the heartbeat width modulation (PWM) method and switch the inverter, the output sign from the current controller is translated from the d-q synchronous references frame to the ABC transformation.

Chapter 03

PI-BASED PSO ALGORITHM

3.1 PI-based PSO algorithm:

The PI controller is often a feedback management loop created using load-primary-based device equations that have been linearized [33]. The major criteria for using PI controllers to control inverter systems are good control performance, seamless implementation, and high reliability. In order to control grid current and intermediate circuit voltage, modern controllers and maximum AC system voltage use PI controllers. By doing so, he is able to stabilize the DC hyperlink voltage of the inverter machine and properly control the active power delivered to the power supply. This is because significant nonlinear effects from inverters and loads lead to device voltages and current harmonics, which completely kill a power device [34]. His PI controller scheme for grid-connected inverters using inductive filters has undergone a lot of development in this area. For instance, in [35], the authors suggested a straightforward, step-by-step controller design technique for grid-tied inverters of the LCL type. We obtain the complete range of details of the controller parameters for assembling the device specification, from which we can easily read the controller parameters, by carefully managing the interaction between the current controller and the energy decay. Additionally, the annualized stability cost of LC filter-equipped grid-connected inverters is calculated [36]. The outcomes of this study demonstrated that when utilizing a typical His PI controller, potential differences in grid impedance have a considerable impact on device stability. Due to its simplicity and balance, PI controllers have traditionally been utilized in synchronous reference frames. Even though PI controllers are incredibly honest when it comes to tuning, the variation in nonlinear load conditions and grid disturbances creates significant obstacles to finding a top-notch and completely durable solution, and relies on the designer to achieve first-rate performance [37]. According to the most recent research, employing focusing commands applied in a three-section inverter device can reduce negative voltage regulation in a grid-linked PV machine with a PI controller [38]. Additionally, the grid-connected inverter device uses

the L-kind clean out, which has been shown to reduce cutting-edge harmonics [39], which is controlled by the finite version predictive. This control strategy, however, necessitates the dimensioning of all device nation variables, adding an additional layer of complexity to the inverter system. In the current study, the PSO algorithm optimization approach is used for the best design of the PI controller parameters to obtain the best and most suitable values of K_p and K_i in real-time operation to decrease the short reaction, reduce time overshoot, and reap low consistent-kingdom errors caused by load variations inside the 3-phase, grid-linked PV inverter device.

By attempting to determine the safest values of K_p and K_i in real time, this is done in order to make sure that the optimization procedure utilizing the PSO algorithm is well-drawn and offers a speedy response. This PSO algorithm optimization method responds right away to fix input mistakes from the device. A possible design for the PSO-based inverter managing equipment is shown in Figure 8. By reducing the error between voltage regulators and cutting-edge regulators, a PSO approach is used to optimally design the parameters of PI regulators. The PSO algorithm's fitness functions and constraints are described in detail below. The parameters of Desk 3 throughout the implementation describe the key advantages and disadvantages of the conventional Ziegler-Nichols approach, fuzzy common sense controller, neural fuzzy common sense, GA, and PSO algorithms. Best response in comparison to other approaches. When compared to fuzzy common sense controllers, PSO algorithms do not require inference rules across implementations, while fuzzy neural expertise necessitates time-consuming trial-and-error methods. the result is

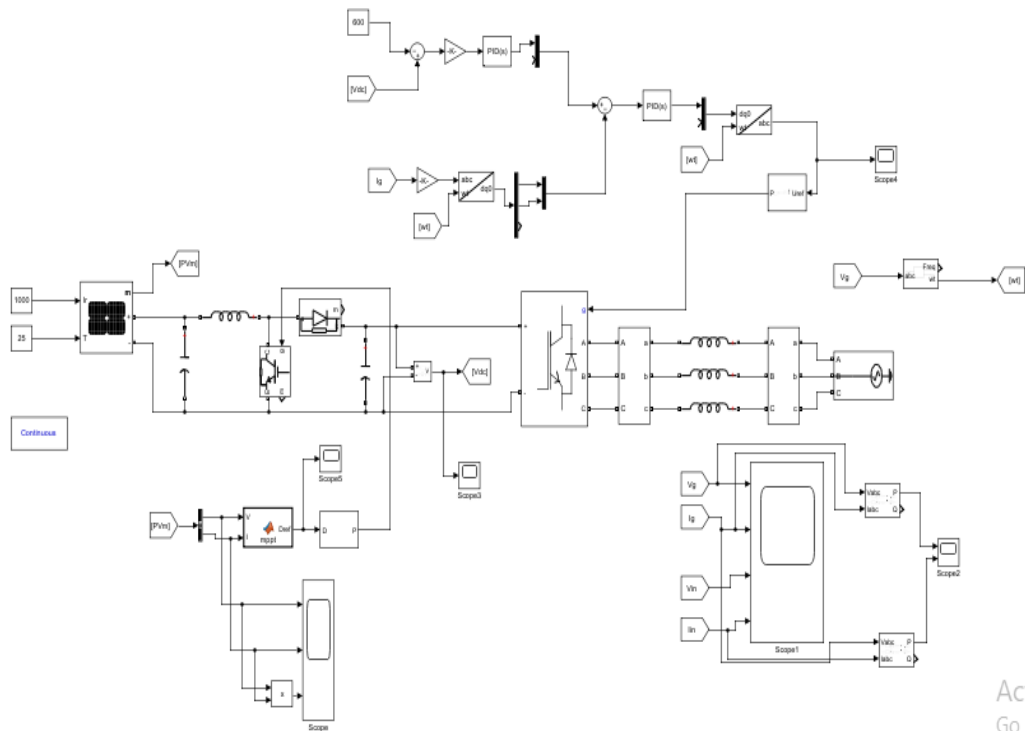


Fig8. Schematic diagram of the proposed PSO optimization technique for the inverter control scheme.

Table3. Advantages and disadvantages of the control algorithm.

Algorithm	Data Training	Rules	Function evaluation	Parameter setting	References
Ziegler-Nichols	No	No	No	Simple with calculation	[6]
Fuzzy Logic controller	No	Yes	No	Simple but trial and error	[7]
Neural Fuzzy Logic	Yes	Yes	No	Huge set of parameters	[9, 11]
GA	No	No	Yes	Huge set of parameters	[12]
PSO	No	No	Yes	Simple set of parameters	[17, 18]

To find the best values of the PI controller settings with quicker replies, use the PSO method, which facilitates an easy and quick implementation procedure with a single solution space.

3.2 Fault Analyses:

A photovoltaic system might experience a variety of defects. Here we list several different types of worrying flaws and strategies to correct them.

1) Ground Fault: A ground fault is an electrical short circuit involving the ground and one or more conductors that are normally labeled as current-carrying conductors. The magnitude of the ground-fault current is influenced by geographical factors, fault impedance, and fault location. If a ground fault is not cleared by proper fault protection, the fault connection may begin to grow and sustain a DC arc, which could pose a fire risk. The following factors frequently contribute to common ground faults [40, 42]:

>> Incidental short circuit between a normal conductor and ground, which occurs when a wire in a junction box for a module accidentally contacts a grounded conductor:

>>>Animals chewing through cable insulation and resulting in a ground fault is an example of cable insulation failure.

>> Ground problems with PV modules, or the shorting out of a solar cell to grounded module frames as a result of a PV module's degrading encapsulation, impact damage, or water corrosion.

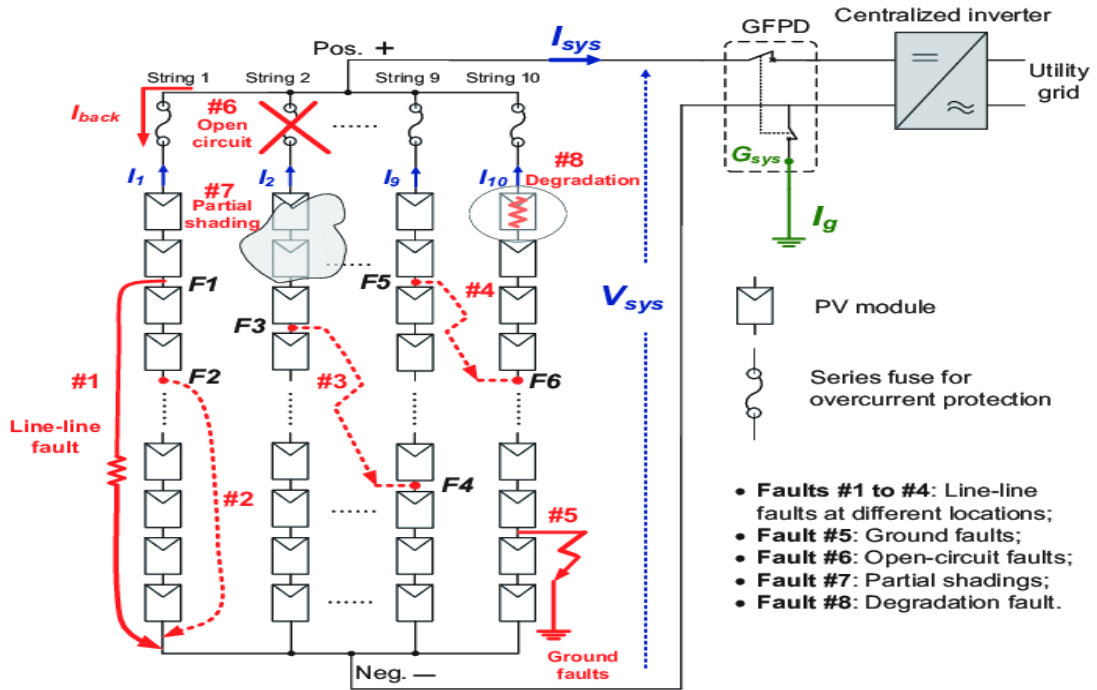


Fig9: Typical-faults-in-a-grid-connected-PV-system

2) Line-to-Line Fault: A line-line fault occurs when two electrically charged sites in a system or network unintentionally form a low-resistance link. A short-circuit fault between PV modules or array cables of different potentials is the conventional definition of a line-line fault in photovoltaic systems. In this study, it is assumed that ground points are not present in line-line faults. A line-line fault could be categorized as a ground fault if it lacks any ground points.

The following are possible root causes of a line-line fault: [42]

>>Accidental short circuit between two conductors that convey current, such as a nail piercing exposed wiring.

>>Animals biting through cable insulation and resulting in a line fault is known as "cable insulation failure."

>> Line-line failures in the DC junction box, such as water damage or mechanical issues.

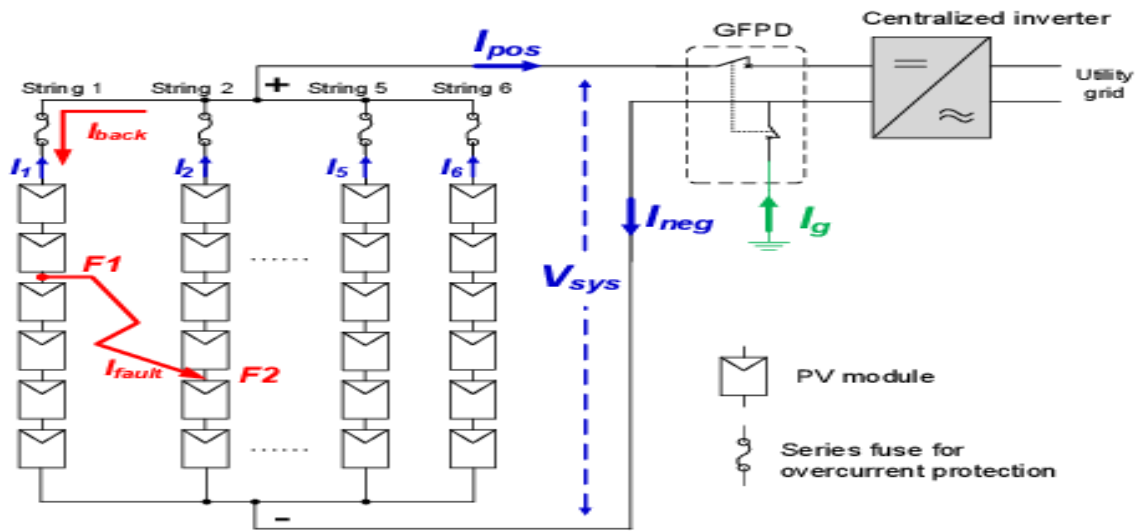


Fig10: Schematic Line to-line fault.

CHAPTER 04

RESULT AND DISCUSSION

4. Results and discussion:

3 MW grid-connected PV power was applied in MATLAB/Simulink with constant irradiance and temperature of 1000 W/m² and 25 W/m², respectively, to apply the suggested PSO for adjusting the PI controller settings in the inverter control scheme. To support the proposed PSO sequence for the inverter operating scheme, we show simulation and test data. The very safe parameter values of the PI regulator, the stark contrast between the results obtained with and without optimization, and his THD of voltage Rated are the key features of the results. The latter demonstrates how his three-part grid-related inverter for PV devices is strengthened by the suggested optimization technique. The performance of the final PI controller parameters for the three-segment grid-connected PV devices is compared in Table 4. To enhance the performance of the inverter device, these parameters are utilized within the inverter controller management algorithm. After a period of trial and error, the initial cost of his PI controller for an inverter machine was altered. His three-part grid-related PV machine version of the MATLAB/Simulink environment simulation is where these trial-and-error values are initially used. The PSO algorithm code is then simulated, and after 100 iterations, the version enters execution mode. The final values of the PI controller are displayed in Table 4 after repeating this procedure up to a maximum of 100 times.

Matlab Code for PSO Based PI Controller:

```
function Dref = mppt(V, I)
Dinit = 0.42;
Dmax = 0.9;
Dmin = 0.1;
delDref = 0.00008;
persistent Vold Pold Drefold;
if isempty(Vold)
    Vold = 0;
```

```

Pold =0;
Drefold=Dinit;

end
P=V*I;
delv=V-Vold;
delp=P-Pold;
if delp>0
    if delv>0
        Dref=Drefold-delDref;
    else
        Dref=Drefold+delDref;
    end
elseif delp<0
    if delv>0
        Dref=Drefold+delDref;
    else
        Dref=Drefold-delDref;
    end
else
    Dref=Drefold;
end

if Dref>Dmax || Dref<Dmin
    Dref=Drefold;
end

Drefold=Dref;
Pold=P;
Vold=V;

```

The intermediate circuit voltage of the PI controller with and without the optimization technique is compared in Figure 11. As can be observed, the PSO technique has a rise time of 0.112 seconds, whereas the PI controller without optimization has a rise time of 0.1322 seconds. By making the DC link voltage more responsive than the conventional PI controller, the goal is to stabilize the inverter machine's DC input voltage. In 0.4 seconds, the grid device's charging process completely changes. Furthermore, the PI controller was able to reach normal landing circumstances more quickly than with a conventional PI controller because to the PSO technique. Consequently, PSO Approach

can eliminate the short circuit effect on the device and give the inverter a steady DC input. The DC hyperlink input stage is stabilized and causes less ripple on the inverter's AC output waveform. Figures 12 and 13 illustrate, respectively, the device with controller's modern outputs and three-phase voltage. A simulation employing a PI regulator with and without PSO technology is used in Figure 12 to evaluate the power supply output voltage.

Table 4. Comparison of the values of the final parameters with different techniques

Item	PI Controller		
	Trial and Error	Ziegler-Nichols	PSO Technique
Proportional gain of voltage regulator, $K_p v$	0.532	2.05	1.4575
Integral gain of voltage regulator, $K_i v$	10	1.56	3.1055
Proportional gain of active current controller, $K_p d$	20	0.32	14.575
Integral gain of active current controller, $K_i d$	250	20	13.105
Proportional gain reactive current controller, $K_p q$	3.052	1.5	0.9226

Integral gain of active current controller, K_i	150	20	16.349
DC link oscillation peak	620.47	599.8	532.12
Frequency, Hz	50	50	50

At $t = 0.4-6$ s, the load step on the grid system suddenly increases, and a slight noise is observed in the voltage amplitude from the conventional PI controller technique. Fig 11 shows that the output voltage from the conventional PI controller has a harmonic waveform at 0.065

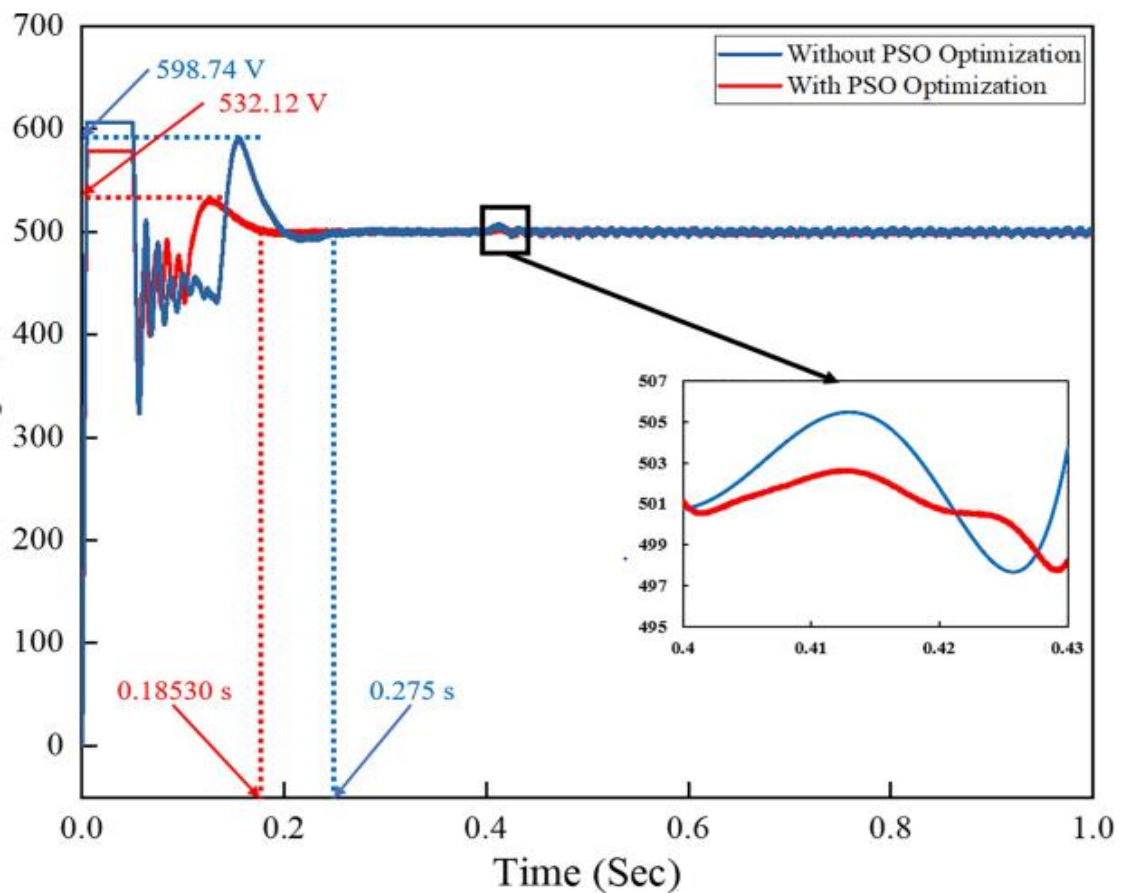


Fig 11. DC link voltage for both the conventional and optimization methods

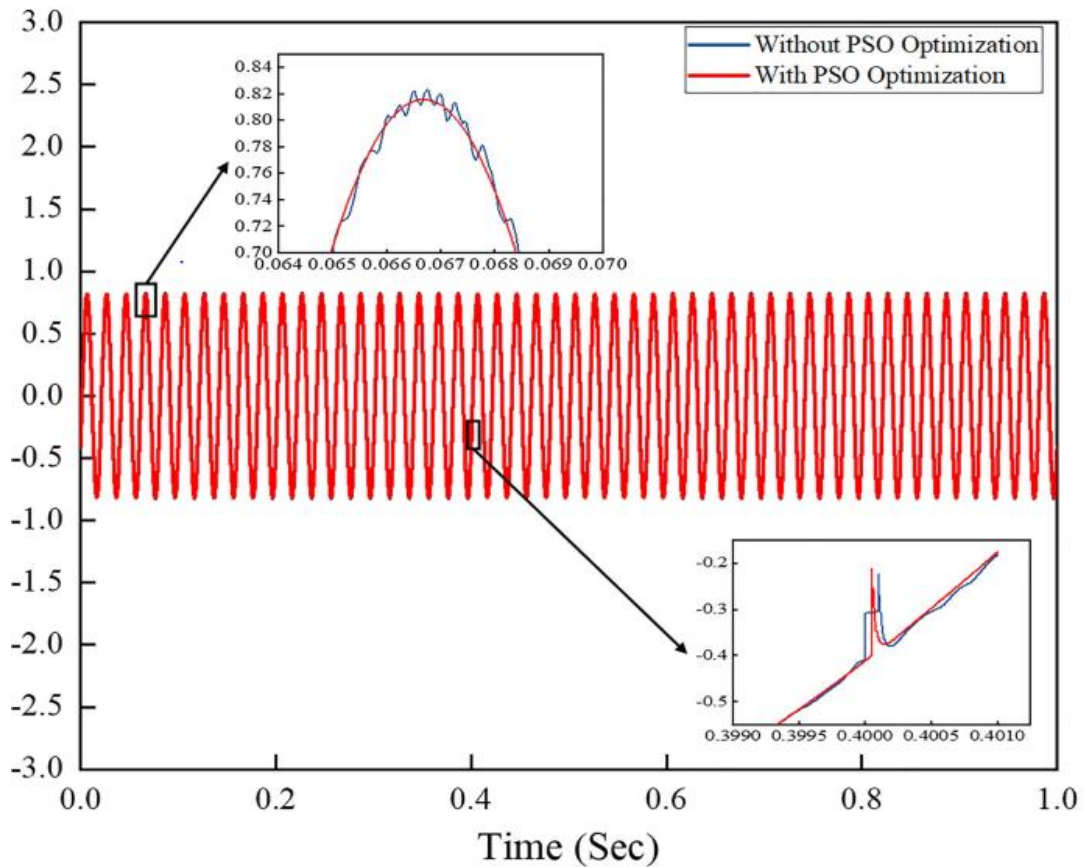


Fig 12. Three-phase output voltage comparison of the output grid system

Compared to the output voltage of the PI regulator utilizing the PSO technique, which has significantly less harmonic output waveforms, 0.07 seconds are required. The inverter operation scheme's proper management algorithms, which reduce the output sign's harmonic levels and offer a constant output voltage across the device, are responsible for this outcome. Over a period of erratic load variations, the amplitude remains steady and constant.

The output current comparison between his traditional PI controller forcing system and a number of different PI controllers using the PSO technique is shown in Figure 13 The findings indicate that unexpected load step trading causes the output to vary between 0.4 and 0.6 seconds. As the load draws greater current from the power supply unit, the current is enough in the system's load change boom. The output waveform harmonics of the PI controller

Without PSO are better than those of the PI controller that uses PSO technology alone.

This finding demonstrates that

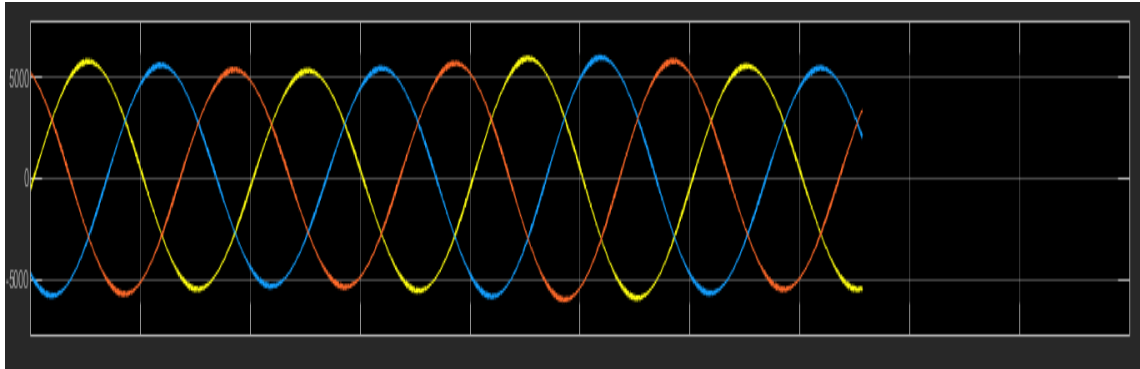


Fig 13. Three-phase output current for the grid system.

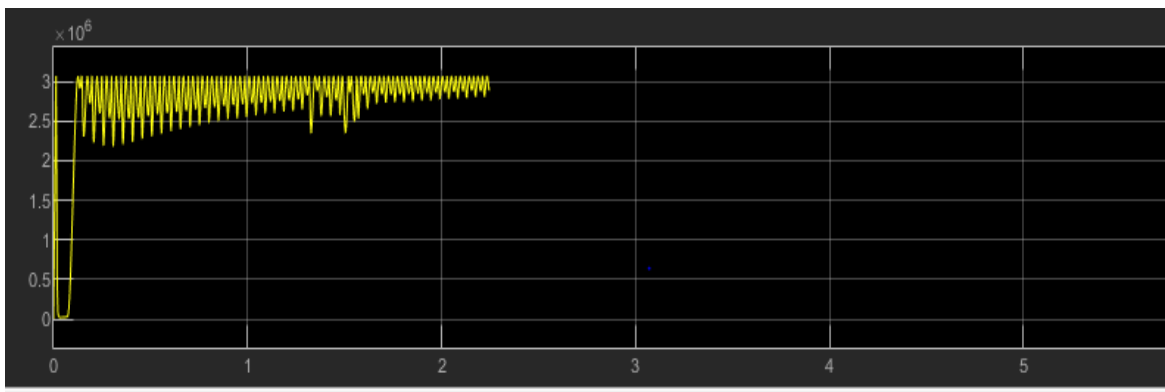


Fig 14. Power flow analysis - PI controller

The potential of inverters is shown in inverters that harvest energy from PV power and supply it to the grid, load demand, and load. Parents have seen that when load requirements are abruptly changed, momentary stumping issues arise. A transition can be used to investigate overshoot. In general, the short-term condition of grid-connected equipment is proportional to insolation power, frequency, and load fluctuations. According to Fig. 14(A), the inverter device exhibits the overshoot in the PV and the grid-delivered energy in the case of a step short in addition to, and showing many transients. This is in contrast to the PSO-based PI controller. In contrast, as seen in Figure 14(B), the PI controller employs the PSO approach to reduce overshoot, lessen the overall transient effect, and return the waist to steady state. As the weight demand rises and falls, a PI controller utilizing the PSO technique can account for device transient effects and overshoot. An important consideration when employing energy devices, especially when connected to the grid, is the machine's optimal performance in terms of voltage and regency with low harmonic content. The explanation is that superior output performance, low THD at voltage, and a cutting-edge signal offer

consumer's greater linear energy, which results in energy savings. The energy component of mass is negatively correlated with the THD issue. An excessive amount of THD components in the line machine are caused by a low power factor consuming the load. His THD problem of voltage and current in the output section may be decreased to an acceptable level of less than 5%, which satisfies the IEEE standard 929-2000 [39, 46], using an upgraded controller and Fast Fourier Transform evaluation. The voltage harmonic spectrum is shown in Fig. 16, and the actual output waveforms from the conventional PI controller and the PSO technique PI controller, respectively, are shown in Fig. 17. The outcome of the harmonic voltage spectrum is zero.

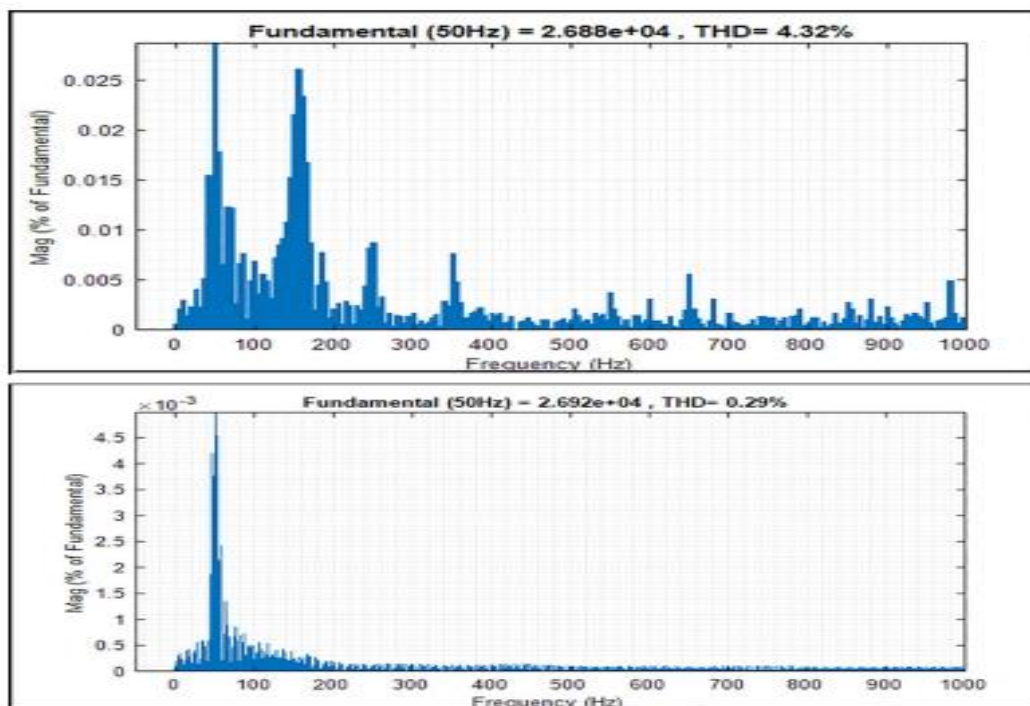


Fig 15. THD and harmonic spectrum of the inverter output voltage.
(a) Conventional PI controller; (b) PI controller with PSO.

PSO approach was used. According to Figs. 15(A) and 15, this represents a reduction of 4.32% compared to the typical PI controller (B). As demonstrated in Fig. 16, the harmonic spectrum of the contemporary on-output inverter machine has values of 4.49 and 2.72% for the traditional PI controller and the PSO technique, respectively. Therefore, improving the inverter machine's controller set of rules results in improved overall device performance. The effectiveness of the suggested controller, which applies the PSO method to the inverter control system with voltage and contemporary controllers, clear out, and sinusoidal PWM approach, is attributed to the harmonic level.

Figure 16 demonstrates that the PSO method minimizes the fitness feature and converges on the price in 48.6 iterations as opposed to the Binary Coded Extremal Optimization (BCEO) rule set, which runs in 68.9 iterations of convergence. It demonstrates arriving at a successful conclusion. Using the PSO rule set, the optimization was carried out for 100 iterations to identify the primes of the generated PI controller parameters K_p and K_i . This PSO is used to determine the voltage and current controllers of the 3-segment inverter device's highest quality values for the PI controller parameters. The PSO technique has a fair overall performance in the controller compared to utilizing the BCEO rule set in the formula to determine the quality value of the PI controller, as can be seen from the results. A grid-connected PV system's frequency behavior utilizing a set of inverter control rules is depicted in Figure 18.

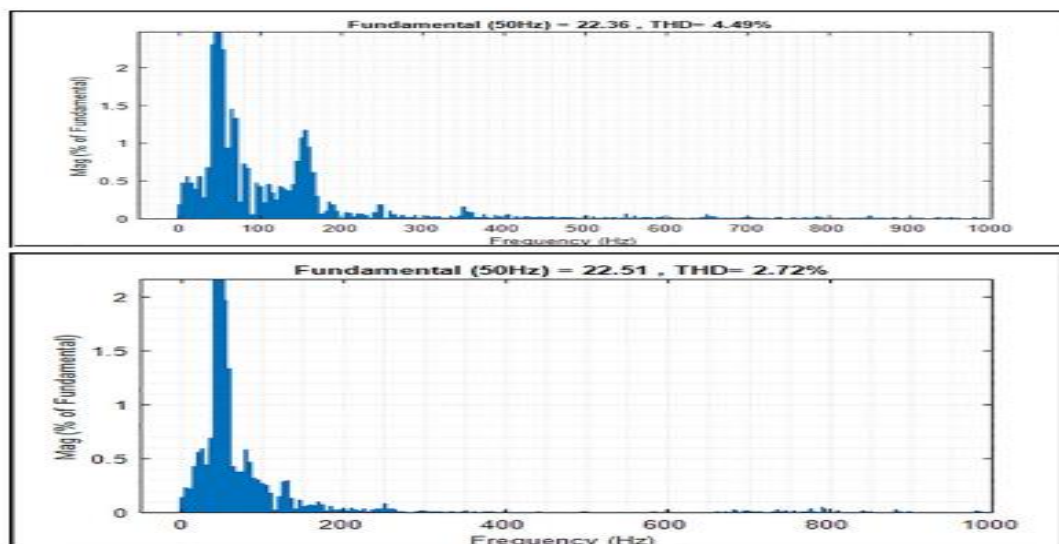


Fig 16. THD and harmonic spectrum of the inverter output current.

(a) Conventional PI controller; (b) PI controller with PSO

Today's big ones are off the net to meet weight demand. The weight demand rapidly reduces at 0.6 seconds, and as a result, the present time is fed back to the grid, resulting in a higher power supply to the load as the load requirement decreases. Compare the frequency response resulting from a PI controller that predominantly uses PSO with a PI controller that doesn't use an optimization procedure. Because the PSO rule defined in the controller accounts for the overshoot during tuning, the frequency response of the PI controller utilizing the PSO approach remains steady and constant during

adjusting the load demand. As previously stated, the voltage regulator controller block determines the identification of the living contemporaneous reference in the d-q axis reference frame and obtains it from the PI controller output using the PSO approach. The analysis of the discovered output curves for the traditional PI controller and the PI controller utilizing the PSO approach is shown in Figure 19. Controlling the i_d or reactive cut-off criterion i_q allows one to regulate the amount of energy and reactive power sent to the grid. In comparison to that identified by traditional PI controllers, the discriminative reference output of PI controllers with PSO is more reliable and consistent.

Additionally, the chaos brought on by software grid gadgets can be utilized to measure ID's overall functionality. Figure 20 depicts Identity's power response after 0.7 seconds of line interruption. Due to transmission line device interference, grid facet voltage and strength are not currently available.

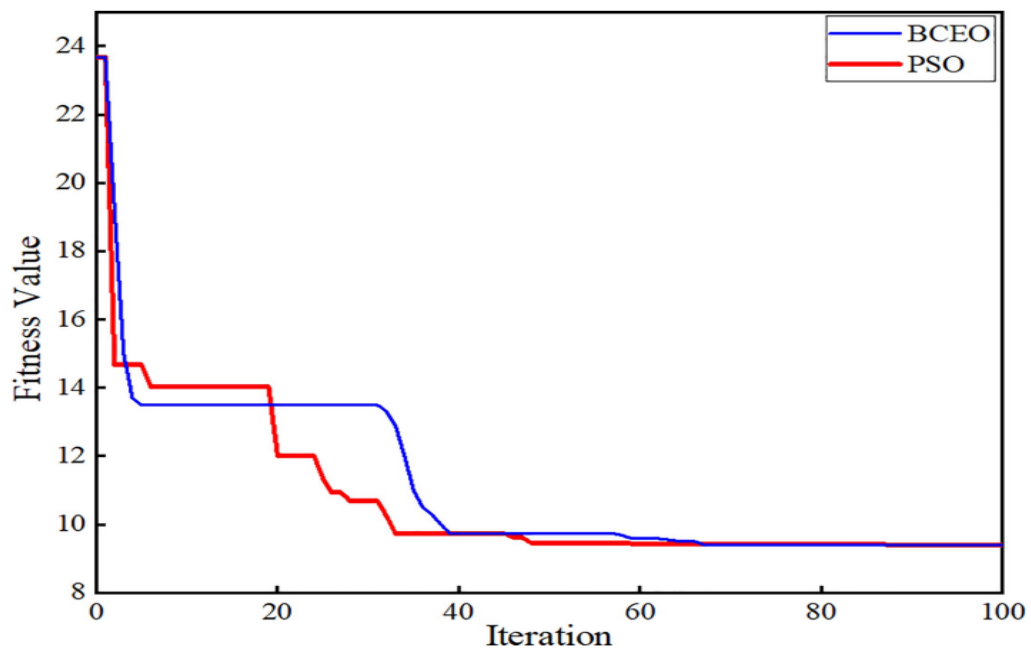


Fig 17. Relationship curve between fitness function and iteration.

When the PSO optimization strategy is used, the reference response of the PI controller is always very powerful and controllable in terms of perturbing the software grid facets. This is so that the device can be charged in the most reliable manner possible using the PSO optimization technique, which can take into account and synchronize any unanticipated disturbances brought on by correct tuning and tweaking of the PI controller settings. In order to provide stable inverter system performance, the PSO

optimization technique is strong and can efficiently regulate his PI controllers in three-phase grid-connected PV inverter devices. The performance comparison between the PSO approach and the conventional PI controller is shown in Table 5. The Ziegler-Nichols approach, the PI-PSO method, the Binary Coded Extremal Optimization (BCEO), and the optimization of the PSO algorithm are the key methods used to compare numerous reported works in this topic. The most popular strategy in control systems is the Ziegler-Nichols approach. A prior study in [40] also demonstrated that the conventional Ziegler-Nichols approach offered superior performance.

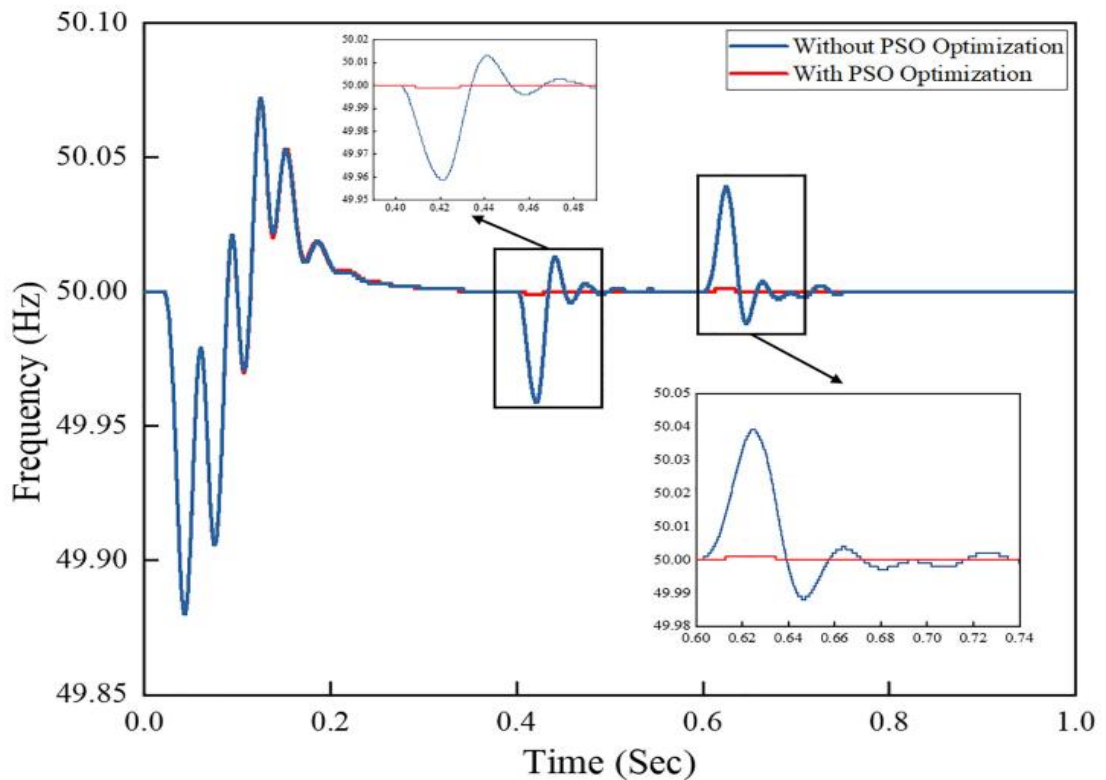


Fig 18. Frequency response of the grid-connected PV system.

A nebulous controller of common sense. As a result, the Ziegler-Nichols method is completely used to determine the typical PI controller strategy. Based on the end period T_u and end gain K_u of the run operating the device in the voltage control loop and inner control loop, the PI controller's peak value is calculated. The final oscillation length and maximum gain are utilized to describe the process dynamics. We can calculate K_p 's value as well as the last period T_u if K_i is assumed to be 0. For PI controllers, the values of such controllers can be found by utilizing the Ziegler-Nichols desk. The progress made in introducing the PSO rule set for gadgets is summarized in Desk 5. The proposed strategy performed better than a number of established techniques, as shown in the table. His PSO technique in this image shows THD to be 0.29 percent for mains voltage and a few 72 percent for current time, respectively, which is lower than values reported in many research. At 0.1853 seconds and 0.112 seconds, respectively, the times to push up and reach constant rich condition are substantially quicker than the others. dual primaries

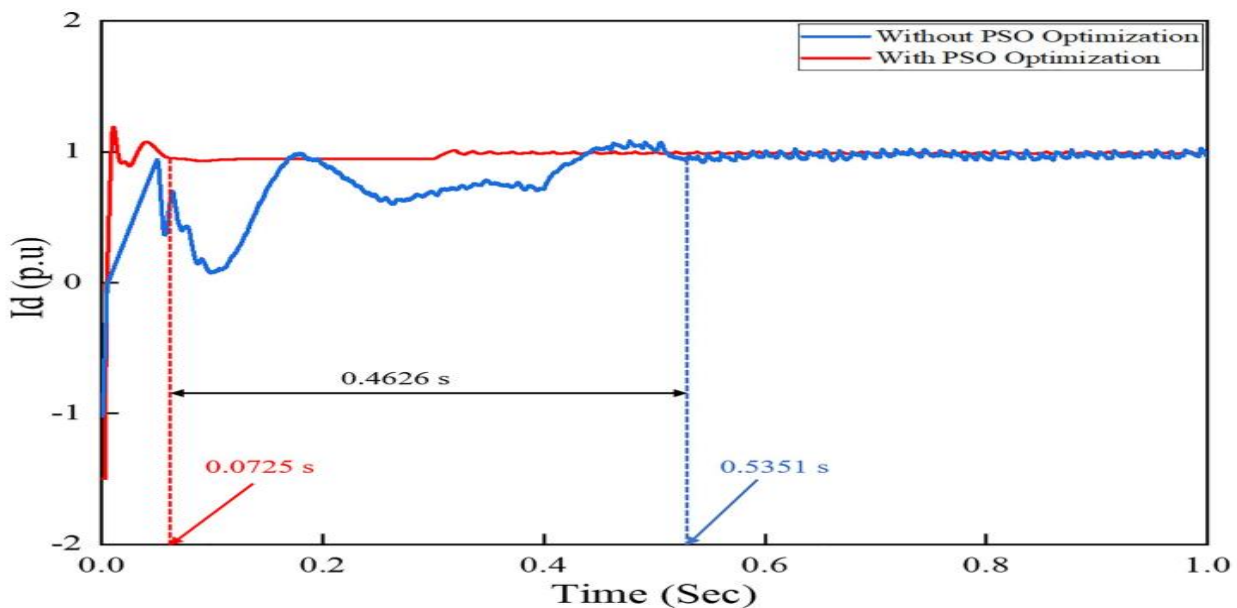


Fig 19. Active current references i_d of the inverter control system under load variation

The variables that lead to the significant improvement in network performance include additional input parameters and optimized input parameters of the control engine. His PSO algorithm for cutting-edge paintings is the voltage loop, reaction force loop, and today's loop with feedforward separation, in comparison to previous works that employed both voltage loops and modern loops most successfully. I'll describe

technology. Within the constraints of the input parameters, the PSO algorithm optimizes each PI controller that is impacted. The optimized input settings of the controller were accepted as a compromise for errors and failures. Based on load variations and grid disturbances, the PSO algorithm tracks faults and fault replacements immediately, giving the controller gold standard value. Due to increased input parameters and optimization-related limitations, the computational error grows. However, it takes time for the PSO ruleset to simulate versions and balance mistakes and alternatives.

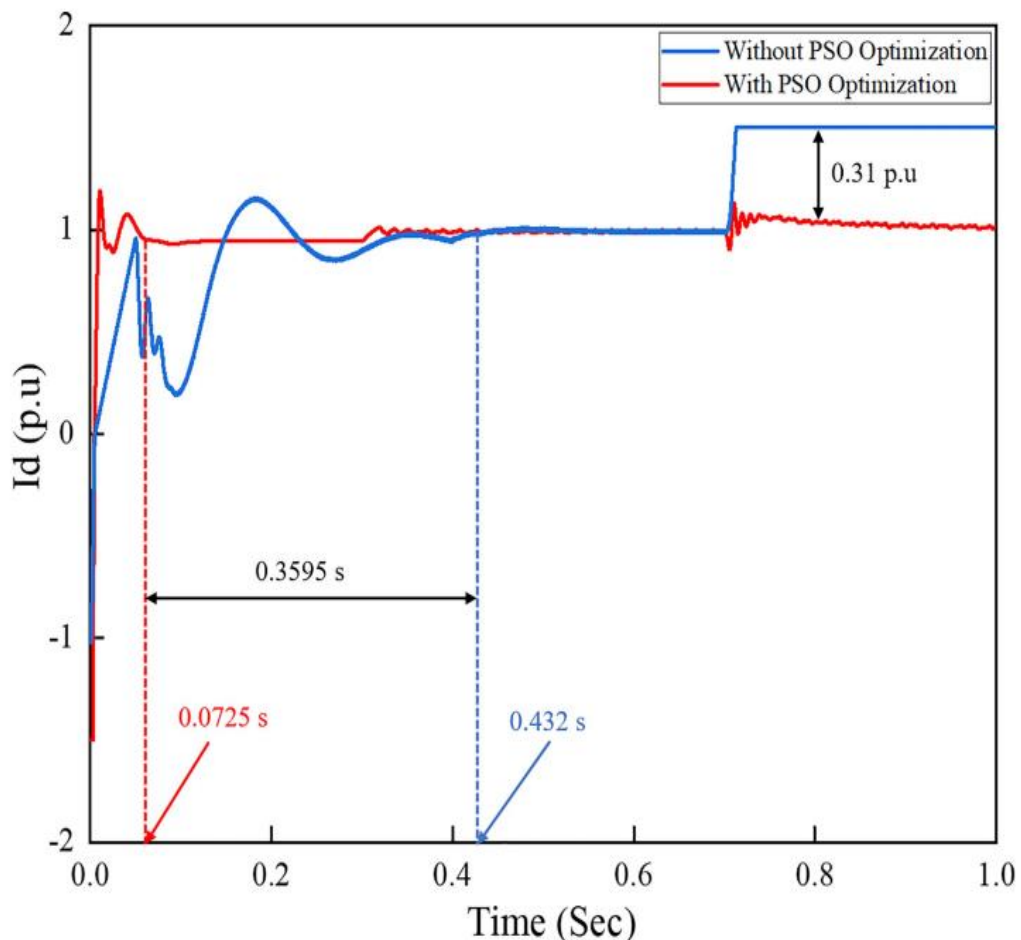


Fig 20. Active current references the id of the inverter control system under grid disturbance.

In comparison to other published work, the rise time needed by the controller to cause a defect in the system was significantly shorter, leading to optimal outcomes and great performance to lower the reference active current of the inverter system. and rapid reactive currents.

CHAPTER 05

CONCLUSION

5 Conclusion:

A controller concept for high-performance control of a three-phase grid-connected PV system is described in this study together with modeling and verification results. The MATLAB/Simulink environment is used to model and test the system. By minimizing the errors in the voltage regulator and current regulator, the PSO approach is used to determine the ideal values of the PI controller parameters. Additionally, to minimize errors as much as feasible, this strategy is adopted.

Table 5. Comparison of reported works.

Item	Pi Controller				
	Ziegler– Nichols [5]	PI-PSO Technique [47]	BCEO-PI controller [48]	PSO Algorithm	Percentage of Improvement from [5, 47, 48] (%)
Total harmonic distortion (%), THD of voltage	4.32	4.20	2.4	0.29	93.2; 93; 87.9
Total harmonic distortion (%), THD of current	4.49	2.9261	N/A	2.72	39.4; 7.04; N/A
Time to reach steady state	0.275	0.38	0.2356	0.1853	32.6; 51.2; 21.3

condition (sec)					
Frequency, (Hz)	50	50	50	50	N/A
Rise time (sec)	0.223	0.3441	0.1652	0.112	49.7; 67.4; 32.2

then ascertain the PI controller's peculiar parameters. Grid disturbances and the effects of load transients are also discussed. In order to minimize error and decrease overshoot, transient response, and control error, the proposed PSO approach establishes the critical PI controller settings and provides the inverter controller with the best possible response. The findings further demonstrate that, in comparison to prior proposed work, the THD probability of the voltage and the actual inverter output signal are substantially lower during load change, at 0.29% and 72%, respectively. Here I am. Additionally, his reaction at typical frequencies below 50Hz is more than 20% faster than the others since it takes much less time (0.1853 seconds) for the input voltage to reach a steady state than the others do.

Finally, the DC link's response time to device fluctuations is 0.112 seconds, which is more than 30% quicker than the other noteworthy results. These outcomes show that by including more useful input factors and optimizing those input parameters, the proposed approach outperforms numerous research papers. In terms of DC-link droop, voltage and current stabilization, harmonic markdown, and frequency stability using this approach, the proposed method exhibits good performance. To achieve sufficient power increase and first-rate strength gains, inverter controller systems in energy equipment applications might employ advanced robust controllers.

Hundreds of individuals experience inconsistent power supply as a result of interruptions in the power produced by PV systems, which are fully dependent on solar radiation. As a result, poor management and an ideal controller design produce pure, cozy, and steady inverter system performance. In order to get the most advantageous settings for the PI controller parameters and enhance device performance for real-time simulation devices, the PSO rule set is therefore executed within the PI controller in this observation

References:

- 1) Ahmed S. et al., “Real-Time Testing of a Fuzzy-Logic-Controller-Based Grid-Connected Photovoltaic Inverter System,” *Renew. Energy*, vol. 5, no. 4, p. 116, 2011, [26/08/2013].
- 2) Hannan M. A., Ghani Z. A., Mohamed A., and Uddin M. N., “Real-Time Testing of a Fuzzy-Logic-Controller-Based Grid-Connected Photovoltaic Inverter System,” *IEEE Trans. Ind. Appl.*, vol. 51, no. 6, pp.4775–4784, 2015, <https://doi.org/10.1109/TIA.2015.2455025>
- 3) Rajesh P., Vais R. I., Yadav S., and Swarup P., “A Modified PI Control for Grid-tied Inverters to Improve Grid Injected Current Quality,” *Int. J. Eng. Technol.*, vol. 9, no. 3, pp. 529–534, 2017, <https://doi.org/10.21817/ijet/2017/v9i3/170903S080>
- 4) Azah Mohamed J. A. A., Hannan M A, “Improved Indirect Field-Oriented Control of Induction Motor DRIVE based PSO Algorithm,” *J. Teknol.*, vol. 2, pp. 19–25, 2016, [Online]. Available: www.jurnalteknologi.utm.my.
- 5) Girirajkumar D. J., S M, “PSO based Tuning of a PID Controller for a High Performance Drilling Machine,” *Int. J. Comput. Appl.*, vol. 1, no. 19, pp. 12–18, 2010.
- 6) Yucelen T., Kaymakci O., and Kurtulan S., *Self-tuning PID controller using Ziegler-Nichols method for programmable logic controllers*, vol. 1, no. PART 1. IFAC, 2006. <https://doi.org/10.1016/j.comppsy.2005.04.005> PMID: 16324902
- 7) Basilio J. C. and Matos S. R., “Design of PI and PID Controllers With Transient Performance Specification,” *IEEE Trans. Educ.*, vol. 45, no. 4, pp. 364–370, 2002.
- 8) Anjum W., Husain A. R., Aziz J. A., Abbas Abbasi M., and Alqaraghuli H., “Continuous dynamic sliding mode control strategy of PWM based voltage source inverter under load variations,” *PLoS One*, vol. 15, no. 2, pp. 1–20, 2020, <https://doi.org/10.1371/journal.pone.0228636> PMID: 32027697
- 9) Ali J. A., Hannan M. A., Mohamed A., and Abdolrasol M. G. M., “Fuzzy logic speed controller optimization approach for induction motor drive using

- backtracking search algorithm,” *Meas. J. Int. Meas. Confed.*, vol. 78, pp. 49–62, 2016, <https://doi.org/10.1016/j.measurement.2015.09.038>
- 10) Jin T., Li P., Zhao L., Du X., and Ma X., “Optimization of Hydrodynamic and Hydrostatic Steering Control System Based on GA-PID,” *2010 Chinese Control Decis. Conf.*, pp. 3180–3184, 2010, <https://doi.org/10.1109/CCDC.2010.5498629>
- 11) SUSATYO HANDOKO S., HADI SASONGKO P., “Parameter Optimization of Proportional Integral Controller In Three-Phase Four-Wire Grid-Connected Inverter Using Ant Colony Optimization,” *J.Theor. Appl. Inf. Technol.*, vol. 73, no. 3, pp. 411–417, 2015.
- 12) song LiJung Huang L., Long Bo, Li Fusheng, “A Genetic-Algorithm-Based DC Current minimization Scheme For Transformerless Grid-Connected Photovoltaic Inverters,” *Energies*, no. february 2020, 2020.
- 13) Besheer A. H. and Adl M. Y., “Ant Colony System Based PI Maximum Power Point Tracking for Stand Alone Photovoltaic System,” *IEEE Conf. Ind. Technollogies*, pp. 693–698, 2012.
- 14) Annamraju A. and Nandiraju S., “Coordinated control of conventional power sources and PHEVs using jaya algorithm optimized PID controller for frequency control of a renewable penetrated power system,” *Prot. Control Mod. Power Syst.*, vol. 4, no. 1, 2019, <https://doi.org/10.1186/s41601-019-0144-2>
- 15) Wang L., Huang C., and Huang L., “Parameter estimation of the soil water retention curve model with Jaya algorithm,” *Comput. Electron. Agric.*, vol. 151, no. July 2017, pp. 349–353, 2018, <https://doi.org/10.1016/j.compag.2018.06.024>
- 16) Ali A. S. O. E. S. and Elazim S. M. A., “PI controller design for MPPT of photovoltaic system supplying SRM via BAT search algorithm,” *Neural Comput. Appl.*, 2015, <https://doi.org/10.1007/s00521-015-2091-9>
- 17) Hannan M. A., Ali J. A., Mohamed A., and Hussain A., “Optimization techniques to enhance the performance of induction motor drives: A review,” *Renew. Sustain. Energy Rev.*, vol. 81, no. June 2017, pp. 1611–1626, 2018, <https://doi.org/10.1016/j.rser.2017.05.240>
- 18) Kakkar S., Ahuja R. K., and Maity T., “Performance enhancement of grid-interfaced inverter using intelligent controller,” *Meas. Control (United*

- Kingdom*), vol. 53, no. 3–4, pp. 551–563, 2020, <https://doi.org/10.1177/0020294019879171>
- 19) Atiq J. and Soori P. K., “Modelling of a grid connected solar PV system using MATLAB/simulink,” *Int. J. Simul. Syst. Sci. Technol.*, vol. 17, no. 41, pp. 45.1–45.7, 2017, <https://doi.org/10.5013/IJSSST.a.17.41.45>
 - 20) Mosalam H. A., Amer R. A., and Morsy G. A., “Fuzzy logic control for a grid-connected PV array through Z-source-inverter using maximum constant boost control method,” *Ain Shams Eng. J.*, vol. 9, no. 4, pp. 2931–2941, 2018, <https://doi.org/10.1016/j.asej.2018.10.001>
 - 21) Al-Shetwi A. Q., Sujod M. Z., and Blaabjerg F., “Low voltage ride-through capability control for single-stage inverter-based grid-connected photovoltaic power plant,” *Sol. Energy*, vol. 159, no. November 2017, pp. 665–681, 2018, <https://doi.org/10.1016/j.solener.2017.11.027>
 - 22) Al-Masri H. M. K., Magableh S. K., Abuelrub A., Saadeh O., and Ehsani M., “Impact of different photo-voltaic models on the design of a combined solar array and pumped hydro storage system,” *Appl. Sci.*, vol. 10, no. 10, 2020, <https://doi.org/10.3390/app10103650>
 - 23) Al-Shetwi A. Q., Hannan M. A., Jern K. P., Mansur M., and Mahlia T. M. I., “Grid-connected renewable energy sources: Review of the recent integration requirements and control methods,” *J. Clean. Prod.*, vol. 253, p. 119831, 2020, <https://doi.org/10.1016/j.jclepro.2019.119831>
 - 24) Ramos-Hernanz J., Uriarte I., Lopez-Guede J. M., Fernandez-Gamiz U., Mesanza A., and Zulueta E., “Temperature based maximum power point tracking for photovoltaic modules,” *Sci. Rep.*, vol. 10, no. 1, pp. 1–10, 2020, <https://doi.org/10.1038/s41598-019-56847-4> PMID: 31913322
 - 25) Bandara K., Sweet T., and Ekanayake J., “Photovoltaic applications for off-grid electrification using novel multi-level inverter technology with energy storage,” *Renew. Energy*, vol. 37, no. 1, pp. 82–88, 2012, <https://doi.org/10.1016/j.renene.2011.05.036>
 - 26) Wu H. and Tao X., “Three phase photovoltaic grid-connected generation technology with MPPT function and voltage control,” *Proc. Int. Conf. Power Electron. Drive Syst.*, pp. 1295–1300, 2009, <https://doi.org/10.1109/PEDS.2009.5385758>

- 27) Arafat M. N., Elrayyah A., and Sozer Y., “An effective smooth transition control strategy using droopbased synchronization for parallel inverters,” *2014 IEEE Energy Convers. Congr. Expo. ECCE 2014*, pp. 3964–3970, 2014, <https://doi.org/10.1109/ECCE.2014.6953940>
- 28) Jumani T. A., Mustafa M. W., and Rasid M., “Optimal Power Flow Controller for Grid-Connected Micro-grids using Grasshopper Optimization Algorithm,” pp. 1–22, 2019, <https://doi.org/10.3390/electronics8010111>
- 29) Farrokhhabadi M., Konig S., Canizares C. A., Bhattacharya K., and Leibfried T., “Battery Energy Storage System Models for Microgrid Stability Analysis and Dynamic Simulation,” *IEEE Trans. Power Syst.*, vol. 33, no. 2, pp. 2301–2312, 2018, <https://doi.org/10.1109/TPWRS.2017.2740163>
- 30) Ashabani S. M., Mohamed Y. A. I., and Member S., “New Family of Microgrid Control and Management Strategies in Smart Distribution Grids—Analysis, Comparison and Testing,” *IEEE Trans. Power Syst.*, vol. 29, no. 5, pp. 2257–2269, 2014, <https://doi.org/10.1109/TPWRS.2014.2306016>
- 31) Rizqiawan A., Hadi P., and Fujita G., “Development of grid-connected inverter experiment modules for microgrid learning,” *Energies*, vol. 12, no. 3, pp. 1–16, 2019, <https://doi.org/10.3390/en12030476>
- 32) Hassan M. A. and Abido M. A., “Optimal design of microgrids in autonomous and grid-connected modes using particle swarm optimization,” *IEEE Trans. Power Electron.*, vol. 26, no. 3, pp. 755–769, 2011, <https://doi.org/10.1109/TPEL.2010.2100101>
- 33) Selamat N. A., Ramih T. O., Abdullah A. R., and Karis M. S., “Performance of PID Controller Tuning based on Particle Swarm Optimization and Firefly Algorithm,” *Int. J. Recent Technol. Eng.*, vol. 8, no. 3S2, pp. 225–230, 2019, <https://doi.org/10.35940/ijrte.c1042.1083s219>
- 34) Ping Y., Qunru Z., Zhirong X. U., Haozhe Y., and Yuanhui Z., “Research on Nonlinear Phenomena of Single-phase H-bridge Inverter,” *IEEE PES Asia Pacific Power Energy Eng.*, pp. 0–5, 2014.
- 35) Active-damping C. C. et al., “Step-by-Step Controller Design for LCL -Type Grid-Connected Inverter with Capacitor-Current Feedback Active Damping,” *IEEE Trans. Power Electron.*, vol. 29, no. 3, pp. 1239–1253, 2014.

- 36) Yang S., Lei Q., Peng F. Z., and Qian Z., “A robust control scheme for grid-connected voltage source inverters,” *IEEE Trans. Ind. Electron.*, vol. 58, pp. 1002–1009, 2010, <https://doi.org/10.1109/APEC.2010.5433380>
- 37) Mosaad M. I., El-raouf M. O. A., Al-ahmar M. A., and Bendary F. M., “Optimal PI controller of DVR to enhance the performance of hybrid power system feeding a remote area in Egypt,” *Sustain. Cities Soc.*, vol. 47, no. February, p. 101469, 2019, <https://doi.org/10.1016/j.scs.2019.101469>
- 38) Vinay Kumar M. and Salma U., “A novel voltage regulation technique for a three phase grid connected photovoltaic system using fuzzy fractional order pi controller,” *J. Adv. Res. Dyn. Control Syst.*, vol. 11, no. 8 Special Issue, pp. 2979–2991, 2019, <https://doi.org/10.35940/ijrte.D8937.118419>
- 39) Nguyen T K. K. H. H., “Finite Control Set–Model Predictive Control with Modulation to Mitigate Harmonic Component in Output Current for a Grid-Connected Inverter under,” *Energies*, 2017, <https://doi.org/10.3390/en10070907>
- 40) Abdolrasol M. G. M., Hannan M. A., and Mohamed A., “PSO optimization for solar system inverter controller and comparison between two controller techniques,” *J. Teknol.*, vol. 78, no. 6–2, pp. 77–83, 2016, <https://doi.org/10.11113/jt.v78.8904>
- 41) Chuang L. Y., Huang H. C., Lin M. C., and Yang C. H., “Particle swarm optimization with reinforcement learning for the prediction of CpG islands in the human genome,” *PLoS One*, vol. 6, no. 6, 2011, <https://doi.org/10.1371/journal.pone.0021036> PMID: 21738602
- 42) Nammalvar P. and Ramkumar S., “Parameter Improved Particle Swarm Optimization Based Direct-Current Vector Control Strategy for Solar PV System,” *Adv. Electr. Comput. Eng.*, vol. 18, no. 1, pp. 105–112, 2018.
- 43) Ghazvinian H. et al., “Integrated support vector regression and an improved particle swarm optimization-based model for solar radiation prediction,” *PLoS One*, vol. 14, no. 5, 2019, <https://doi.org/10.1371/journal.pone.0217634> PMID: 31150467
- 44) Valle Y., Member S., Venayagamoorthy G. K., Member S., and Harley R. G., “Particle Swarm Optimization: Basic Concepts, Variants and Applications in

- Power Systems,” *IEEE Trans. Evol. Comput.*, vol. 12, no. 2, pp. 171–195, 2008.
- 45) Dolara A., Grimaccia F., Mussetta M., Ogliari E., and Leva S., “An evolutionary-based MPPT algorithm for photovoltaic systems under dynamic partial shading,” *Appl. Sci.*, vol. 8, no. 4, 2018, <https://doi.org/10.3390/app8040558>
- 46) IEEE Standards Coordinating Committee 21 on Fuel Cells Photovoltaics Dispersed Generation and Energy Storage, *IEEE Recommended Practice for Utility Interface of Photovoltaic (PV) Systems*, vol. 2000. 2000.
- 47) Fahad S., Mahdi A. J., Tang W. H., Huang K., and Liu Y., “Particle Swarm Optimization Based DC-Link Voltage Control for Two Stage Grid Connected PV Inverter,” *2018 Int. Conf. Power Syst. Technol. POWERCON 2018—Proc.*, no. 201807100000006, pp. 2233–2241, 2019, <https://doi.org/10.1109/POWERCON.2018.8602128>
- 48) Dai Y. X., Wang H., and Zeng G. Q., “Double Closed-Loop PI Control of Three-Phase Inverters by Binary-Coded Extremal Optimization,” *IEEE Access*, vol. 4, pp. 7621–7632, 2016, <https://doi.org/10.1109/ACCESS.2016.2619691>